

Polar comonomers regulate and control the copolymerization of conjugated dienes and methoxystyrenes catalyzed by CGC-tape rare-earth metal catalyst

Zhijie Fu^a, Chuang Song^a, Yuanxia Qi^a, Jingting Pei^a, Xuanren Zhu^a, Yanan Zhao^{*b}, Yi Luo^c, Xiaofang Li^{*a}

^a Key Laboratory of Cluster Science of Ministry of Education, Beijing Key Laboratory of Photoelectronic/Electrophotonic Conversion Materials, School of Chemistry and Chemical Engineering, Beijing Institute of Technology, Beijing 100081, China. ^b State Key Laboratory of Organometallic Chemistry, Shanghai Institute of Organic Chemistry, Chinese Academy of Sciences, Shanghai 200032, China. ^c PetroChina Petrochemical Research Institute, Beijing, 102206, China. ^ae-mail: fuxu8805@163.com; eternity973@163.com; qiyuanxia2020@163.com; 18810780713@163.com; 1269260432@qq.com. ^ce-mail: luoyi010@petrochina.com.cn. ^{*b}e-mail: yananzhao99@sioc.ac.cn. ^{*a}e-mail: xfli@bit.edu.cn.

Materials and methods.....	1
Synthesis procedures	2
Computational details	2
Additional spectra.....	3
Rheological measurements	36
Table S1 polymerization of 2,5-FMOS by the complex Y/Al ^t Bu ₃ /[Ph ₃ C][B(C ₆ F ₅) ₄] ternary system.....	37
Copolymerization reactivity ratios and intermittent experiment.....	38
Mechanism of copolymerization of IP and 2,5-FMOS	41
Reference	41

Materials and methods

All manipulations were performed under a dry and N₂-filled atmosphere using standard high vacuum Schlenk techniques or in a MBRAUN LAB star glove box. All solvents were purified via a solvent purification system. Isoprene, Myrcene, Ocimene, *ortho*-methoxystyrene (*o*MOS), *meta*-methoxystyrene (*m*MOS), *para*-methoxystyrene (*p*MOS) were purchased from Energy Chemistry. [Ph₃C][B(C₆F₅)₄], LnCl₃ (Ln=Sc, Y, Lu) were purchased from Aldrich. The Al^tBu₃ (1.0 M solution in toluene) were purchased from Energy Chemical. All the monomers and polar monomers were dried over NaH stirring for 48 hours and distilled before use. The deuterated solvents benzene-*d*6 (99.6 atom% D), chloroform-*d*1 (99.8 atom% D), 1,1,2,2-tetrachloroethane-*d*2 (99.6 atom% D) were obtained from Cambridge Isotope. Organometallic samples for NMR spectroscopic measurements were prepared in the glove box by use of NMR tubes sealed by paraffin film. ¹H, ¹³C NMR spectra were recorded on a Bruker AV400 (FT, 400 MHz for ¹H; 100 MHz for ¹³C) or AV700 (FT, 700 MHz for ¹H; 175 MHz for ¹³C). The molecular weight (*M_n*) and molecular weight distribution (*M_w/M_n*) of the polymers were measured by means of gel permeation chromatography (GPC) on a PL-GPC 220 type high-temperature chromatography equipped with three PL-gel 10 μm Mixed-B LS type columns at 150 °C. Differential scanning calorimetry (DSC) analyses were carried out on a DSC 1 from METTLER-TOLEDO Instruments under a nitrogen atmosphere at a heating rate of 10 °C/min. The thermal history difference in the polymers was eliminated by first heating the specimen to 300 °C, cooling at 10 °C /min to 25 °C, and then recording the second

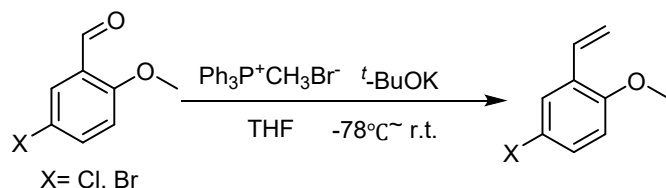
DSC scan from 25 °C to 300 °C at 10 °C/min. All the rheological measurements were performed on Physica MCR-92 System equipped with a 25 mm parallel plate geometry and a gap width of approximately 1 mm in nitrogen at 180 °C and $\gamma = 10\%$. The temperature was controlled with an accuracy of ± 1 °C.

Synthesis procedures

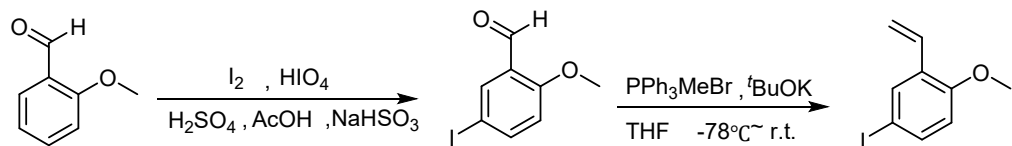
5-fluoro-2-methoxystyrene: According to literature procedures.¹

5-chloro-2-methoxystyrene: Methyltriphenylphosphonium bromide (10.0 mmol) was added to a solution of potassium *t*-butoxide (11.0 mmol) in THF (50 mL). The resulting reaction mixture turned bright yellow and was stirred for 1 h after which, it was cooled to -78 °C. 5-chloro-2-methoxybenzaldehyde (13.0 mmol) was dissolved in THF (10 mL) and added to the reaction which was stirred for 24 h. The reaction was warmed to r.t., diluted with ether and filtered through celite. The filtrate was washed with brine, dried over magnesium sulfate, filtered and concentrated. Silica gel chromatography eluting with 15 % EtOAc/hexanes yielded the desired product, yield 84 %.

5-bromo-2-methoxystyrene: The process was the same as 5-chloro-2-methoxystyrene, yield 82 %.



5-iodo-2-methoxystyrene: The first step to synthesis of 5- chloro-2-methoxybenzaldehyde is according to literature procedures.² Next step was the same as 5-chloro-2-methoxystyrene, afforded pale yellow liquid, yield 76 %.



Computational details

All calculations were performed with the Gaussian 16 program.³ The B3PW91 hybrid exchange-correlation functional was utilized for geometry optimization.⁴⁻⁶ Each optimized structure was subsequently analyzed by harmonic vibration frequencies for characterization of a minimum ($N_{\text{imag}} = 0$) or a transition state ($N_{\text{imag}} = 1$) and providing thermodynamic data. The transition state structures are shown to connect the reactant and product on either side via intrinsic reaction coordinate (IRC) following. The 6-31G* basis set was considered for C, H, O, N, F atoms. The Y and Si atoms were treated by the Stuttgart/Dresden effective core potential (ECP) and the associated basis sets.⁷⁻⁹ The basis sets of Si were augmented with one *d*-polarization function (exponent of 0.284).¹⁰ All optimizations were carried out in the gas phase without any symmetry constraint. The transition state structures are shown to connect the reactant and product on either side via intrinsic reaction coordinate (IRC) following. This basis set is denoted as “BSI”. Such a computational strategy has been widely used for the study of transition-metal containing systems.¹¹⁻¹⁴ To obtain more reliable relative energies, the single-point calculations of optimized structures were carried out at the level of M06^{15, 16}/BSII, taking into account solvation effect of toluene with the SMD¹⁷ solvation model. In the BSII, the 6-311G (d, p) basis set was used for nonmetal atoms, while the basis sets together with associated pseudopotentials for Y atoms are the same as that in geometry optimization. Therefore, unless otherwise mentioned, the free energy (ΔG , 298.15 K, 1 atm) in solution, which was used for description of energy profiles, was obtained from the solvation single-point calculation and the gas-phase Gibbs free energy correction. The 3D molecular structures displayed in this paper were drawn by using CYL view.¹⁸

Additional spectra

NMR spectrums of 5-halide-2-methoxystyrenes

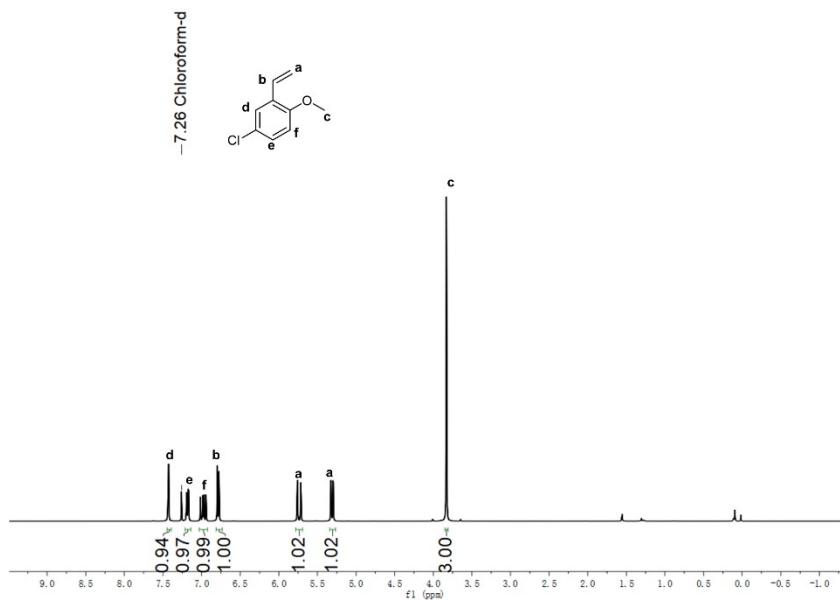


Figure S1. ¹H NMR spectrum of 2,5-ClMOS (400 MHz, CDCl₃): δ 7.43 (d, *J* = 2.6 Hz, 1H), 7.18 (dd, *J* = 8.7, 2.6 Hz, 1H), 6.98 (dd, *J* = 17.7, 11.1 Hz, 1H), 6.79 (d, *J* = 8.8 Hz, 1H), 5.74 (dd, *J* = 17.7, 1.0 Hz, 1H), 5.31 (dd, *J* = 11.1, 0.9 Hz, 1H), 3.83 (s, 3H).

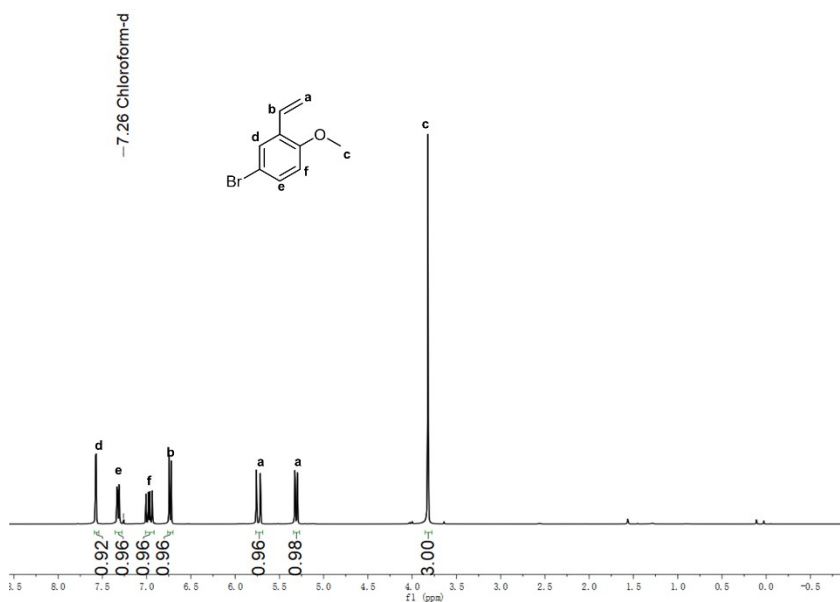


Figure S2. ¹H NMR spectrum of 2,5-BrMOS (400 MHz, CDCl₃): δ 7.57 (d, *J* = 2.4 Hz, 1H), 7.32 (dd, *J* = 8.7, 2.4 Hz, 1H), 6.97 (dd, *J* = 17.7, 11.1 Hz, 1H), 6.73 (d, *J* = 8.7 Hz, 1H), 5.74 (dd, *J* = 17.7, 1.1 Hz, 1H), 5.31 (dd, *J* = 11.1, 1.1 Hz, 1H), 3.82 (s, 3H)

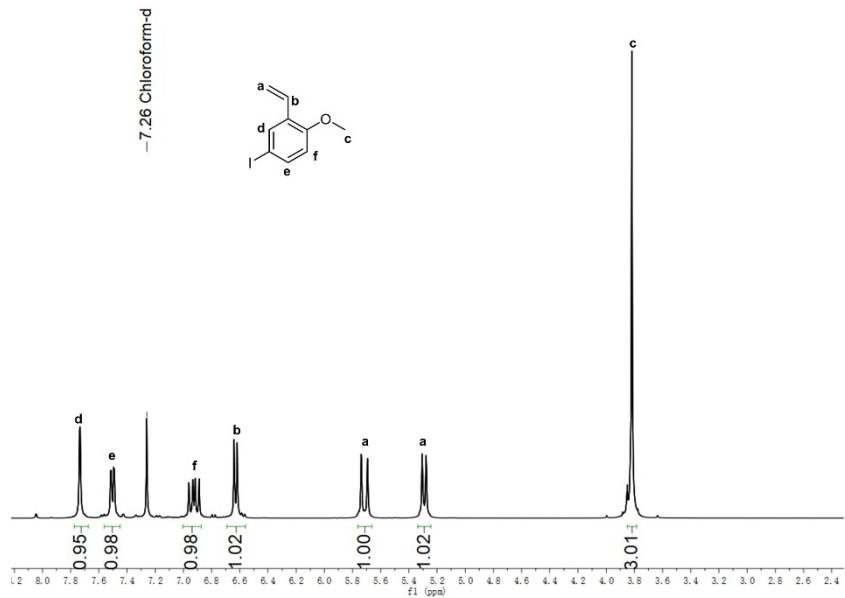


Figure S3. ¹H NMR spectrum of 2,5-IMOS (400 MHz, CDCl₃): 7.50 (dd, *J* = 8.6, 2.0 Hz, 1H), 6.92 (dd, *J* = 17.7, 11.2 Hz, 1H), 6.63 (d, *J* = 8.6 Hz, 1H), 5.75 – 5.68 (m, 1H), 5.29 (d, *J* = 11.1 Hz, 1H), 3.82 (s, 3H).

NMR spectrums of complexes Y

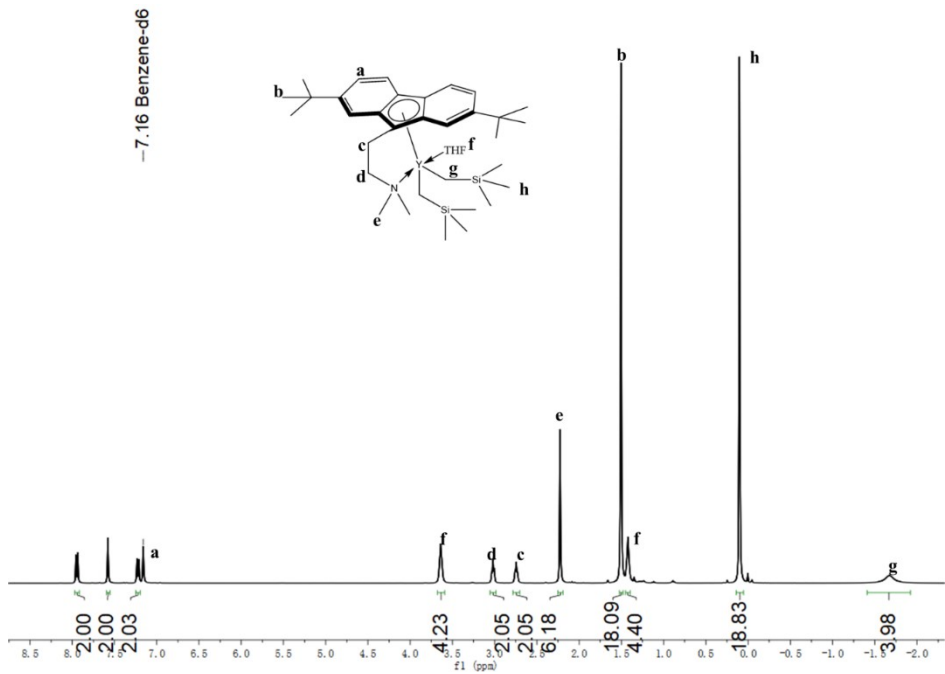


Figure S4. ¹H NMR spectrum of yttrium complex Y (400 MHz, C₆D₆): δ 7.95 (d, *J* = 8.7 Hz, 2H, Aryl), 7.58 (s, 2H, Aryl), 7.22 (d, *J* = 8.6 Hz, 2H, Aryl), 3.64 (s, 4H, THF), 3.02 (t, *J* = 6.0 Hz, 2H, -CH₂-), 2.74 (t, *J* = 5.8 Hz, 2H, Flu-CH₂-), 2.23 (s, 6H, -NMe₂), 1.51 (s, 18H, -^tBu₂), 1.42 (s, 4H, THF), 0.10 (s, 18H, -Si(Me)₃), -1.67 (s, 4H, Y-CH₂-).

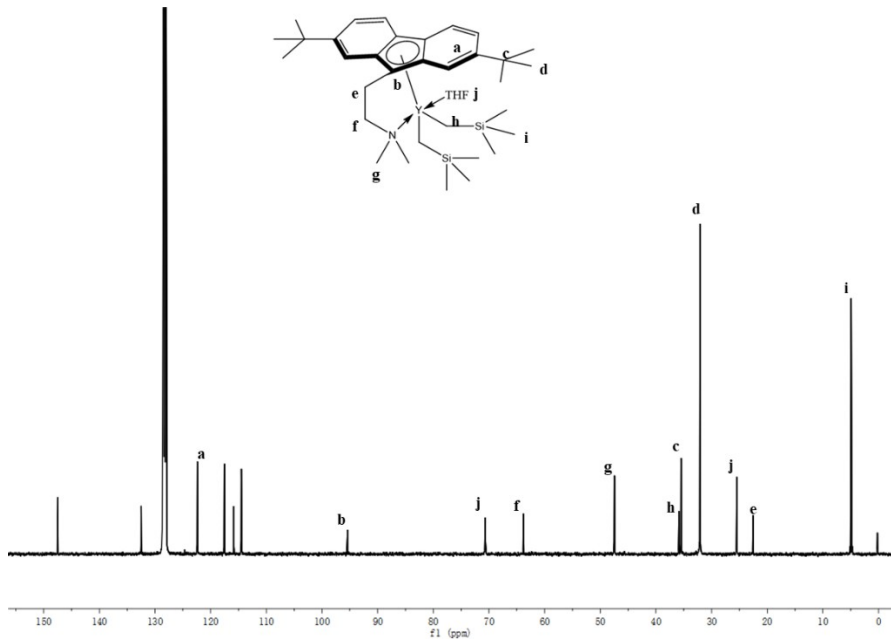


Figure S5. ^{13}C NMR spectrum of yttrium complex **Y** (175 MHz, C_6D_6): δ 147.26 (s), 132.31 (s), 122.20 (s), 117.36 (s), 115.67 (s), 114.31 (s), 95.24 (s), 70.47 (s), 63.62 (s), 47.29 (s), 35.69 (s), 35.29 (s), 31.88 (s), 25.30 (s), 22.36 (s), 4.74 (s).

NMR spectrums of copolymers P(CDs-*co*-PO)s

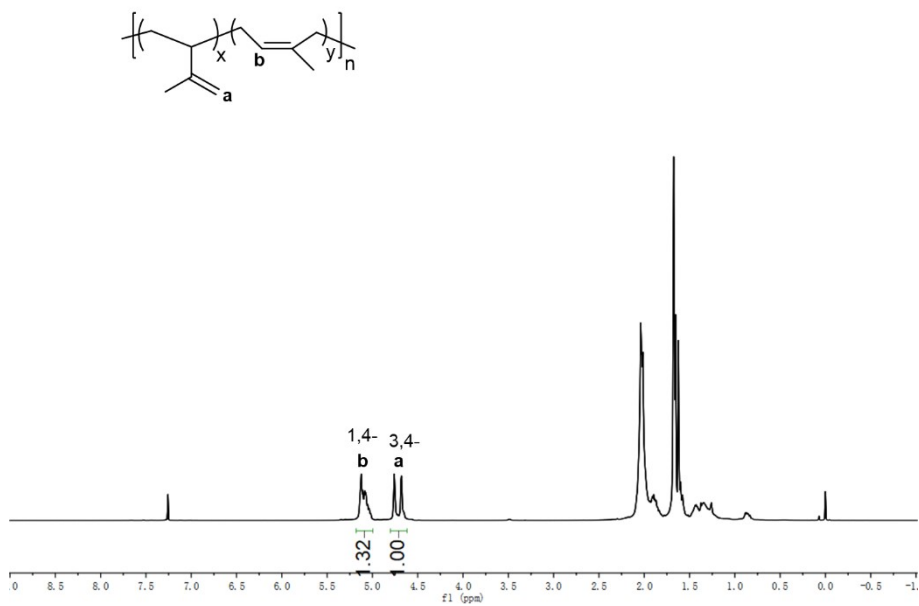


Figure S6. ^1H NMR spectrum of PIP (CDCl_3 , 25°C) in Table 1, entry 1.

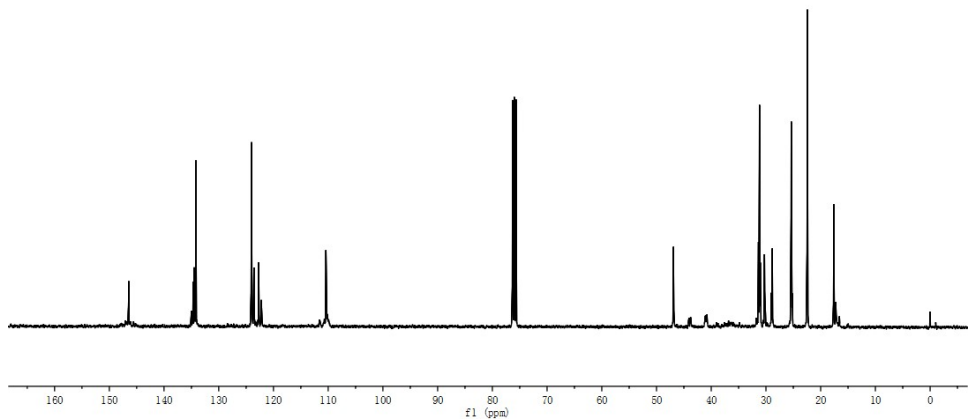


Figure S7. ¹³C NMR spectrum of PIP (CDCl₃, 25°C) in Table 1, entry 1.

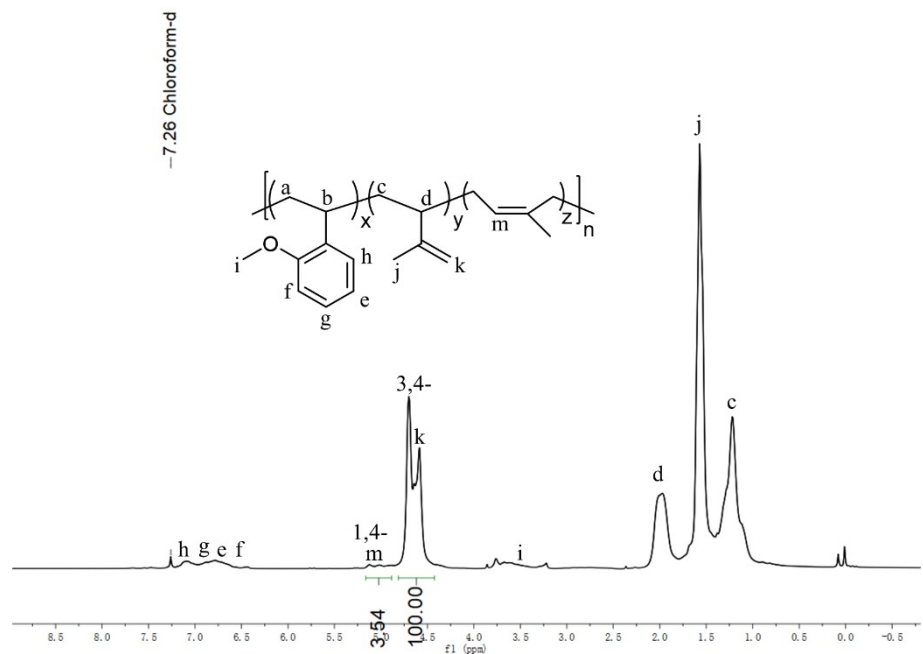


Figure S8. ¹H NMR spectrum of P(*o*MOS-*co*-IP) (CDCl₃, 25°C) in Table 1, entry 2.

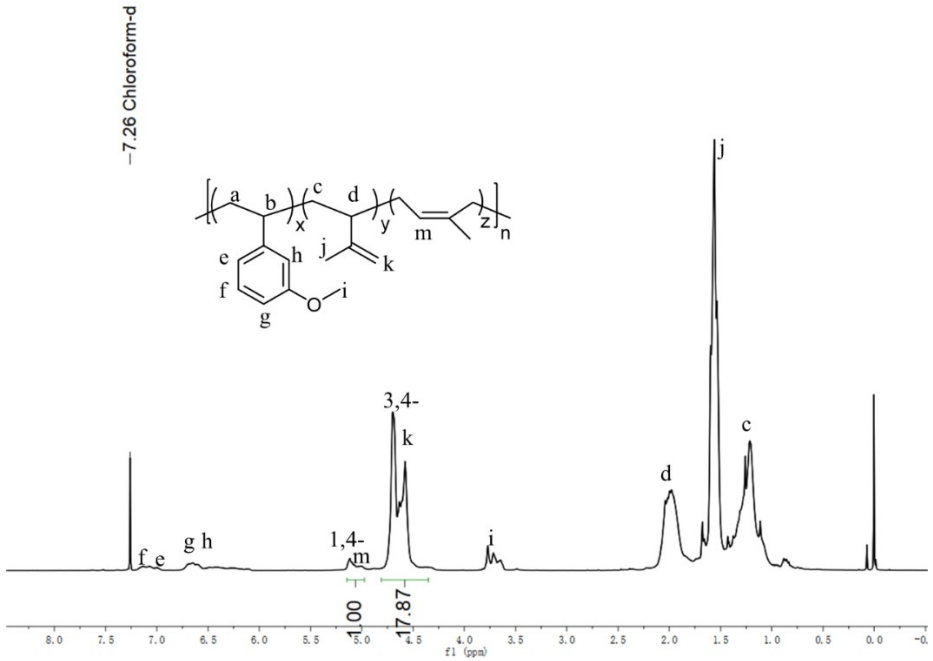


Figure S9. ^1H NMR spectrum of P(*m*MOS-*co*-IP) (CDCl_3 , 25°C) in Table 1, entry 3.

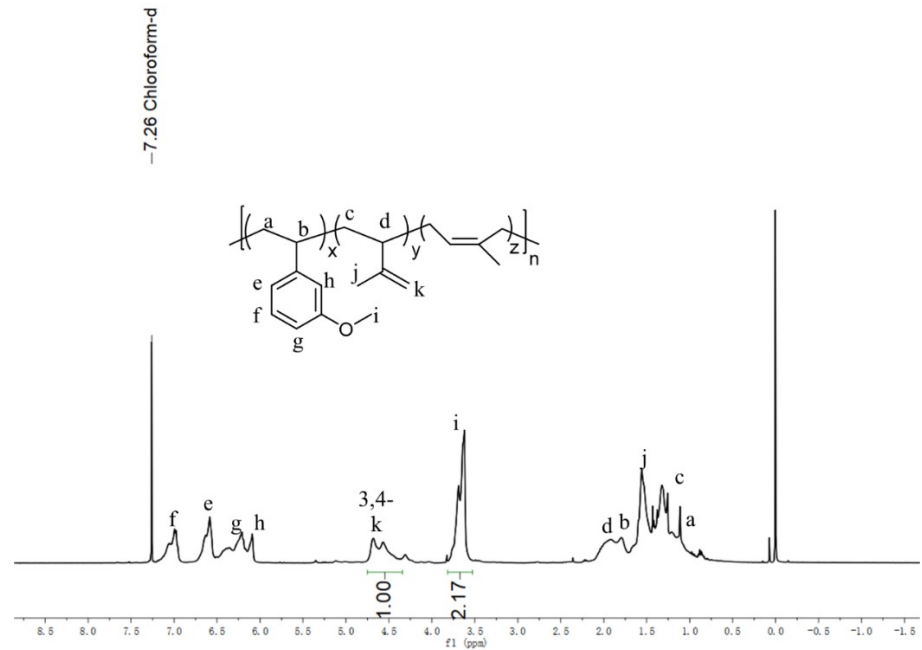


Figure S10. ^1H NMR spectrum of P(*m*MOS-*co*-IP) (CDCl_3 , 25°C) in Table 1, entry 4.

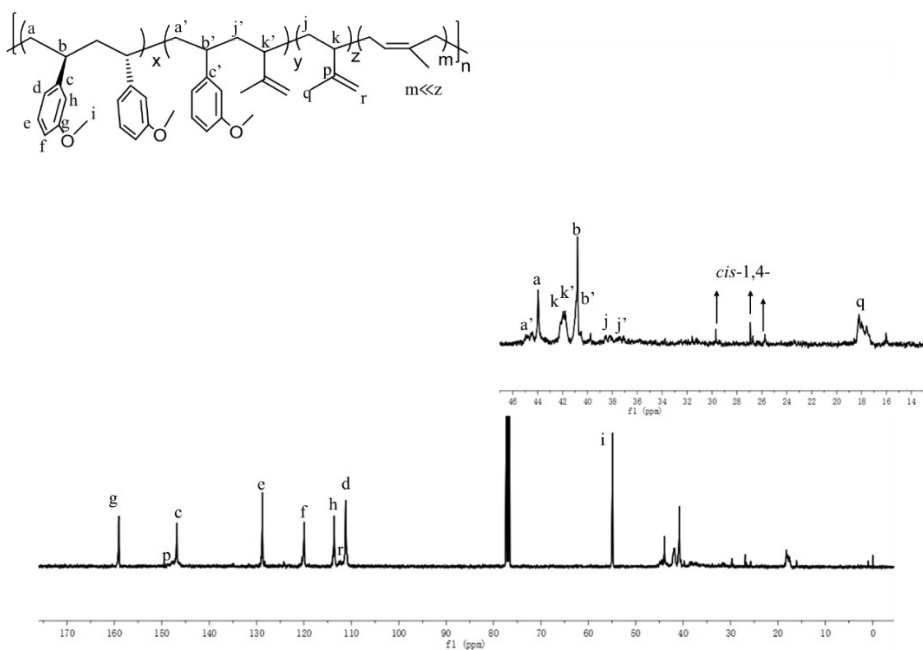


Figure S11. ^{13}C NMR spectrum of P(*m*MOS-*co*-IP) (CDCl_3 , 25°C) in Table 1, entry 3.

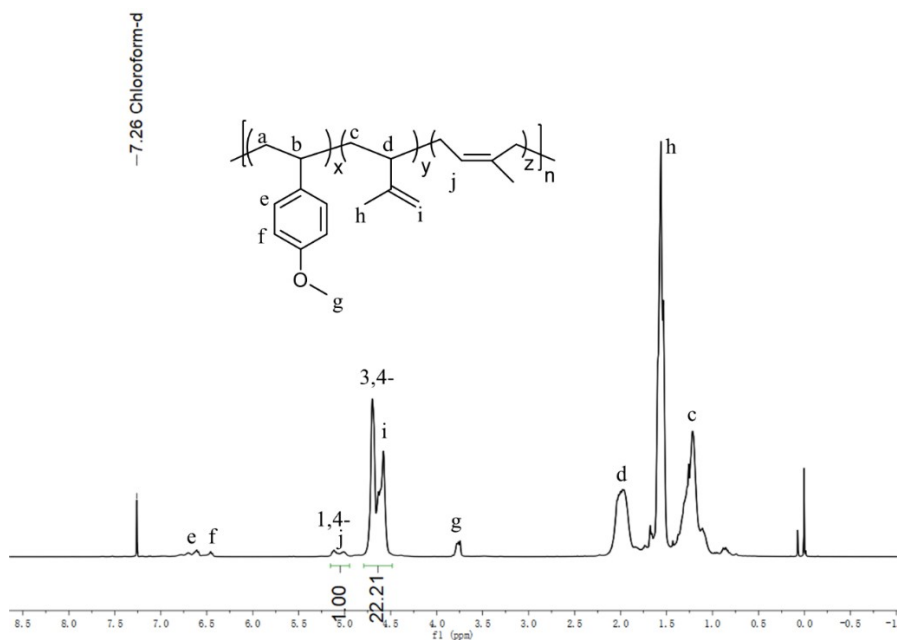


Figure S12. ^1H NMR spectrum of P(*p*MOS-*co*-IP) (CDCl_3 , 25°C) in Table 1, entry 5.

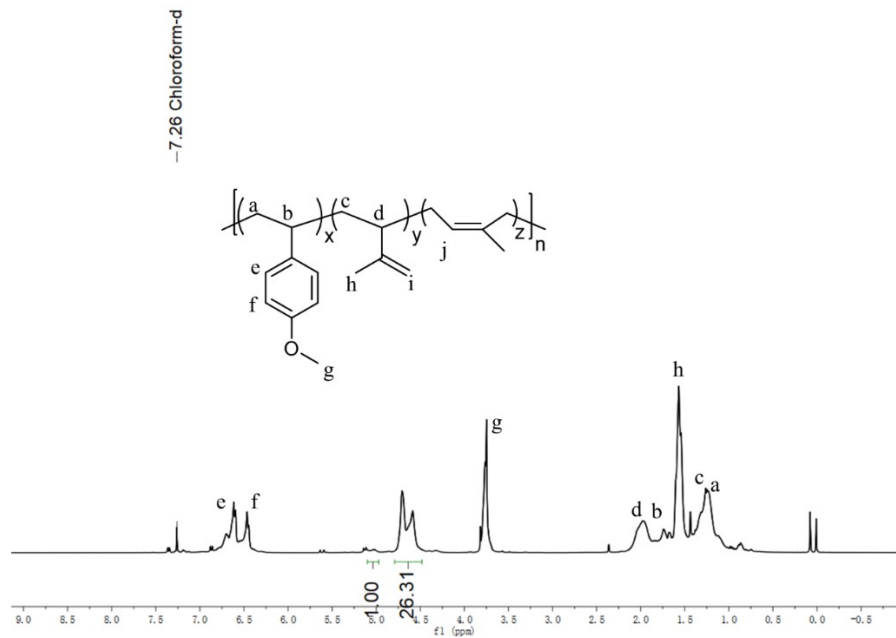


Figure S13. ¹H NMR spectrum of P(*p*MOS-*co*-IP) (CDCl₃, 25°C) in Table 1, entry 6.

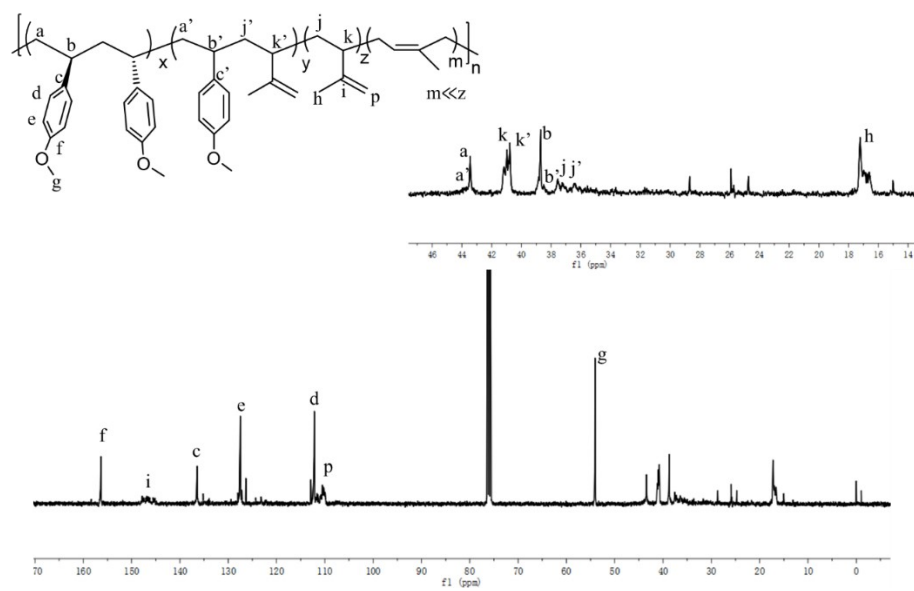


Figure S14. ¹³C NMR spectrum of P(*p*MOS-*co*-IP) (CDCl₃, 25°C) in Table 1, entry 6.

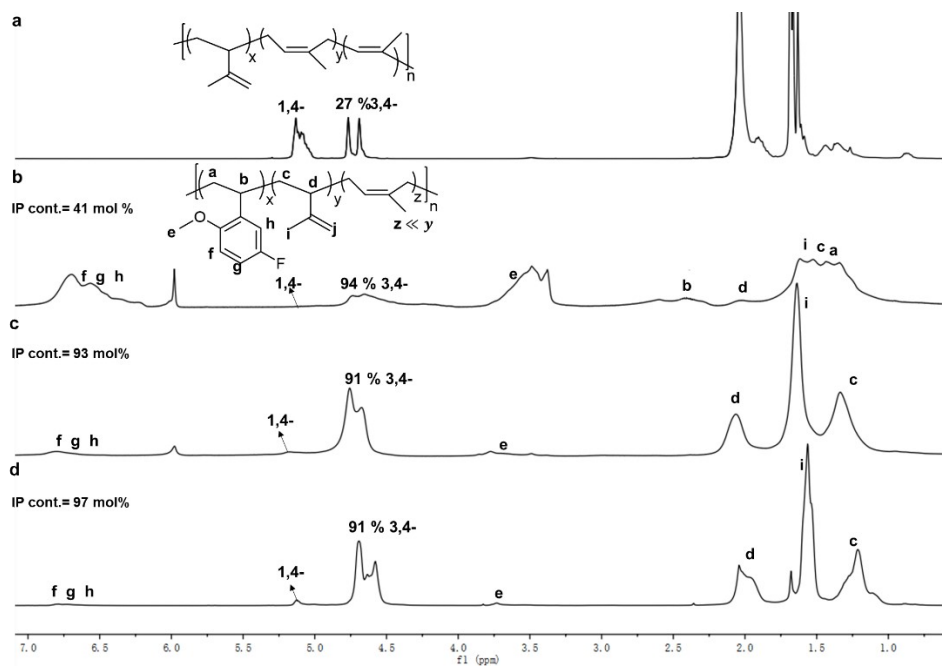


Figure S15. ^1H NMR spectrum of P(2,5-FMOS-co-IP)s. (a) 27 % 3,4- in PIP (CDCl_3 , 25°C) (Table 1, entry 1). (b) 94 % 3,4- in copolymer ($\text{C}_2\text{D}_2\text{Cl}_4$, 110°C) (Table 1, entry 15). (c) 91 % 3,4- in copolymer ($\text{C}_2\text{D}_2\text{Cl}_4$, 110°C) (Table 1, entry 10). (d) 91 % 3,4- copolymer (CDCl_3 , 25°C) (Table 1, entry 9).

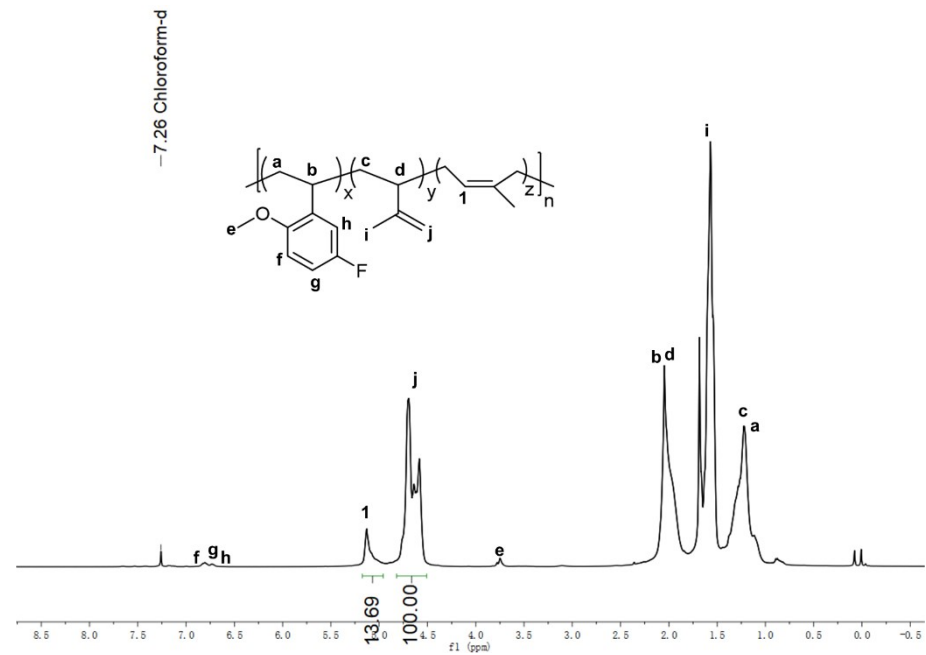


Figure S16. ^1H NMR spectrum of P(2,5-FMOS-co-IP) (CDCl_3 , 25°C) in Table 1, entry 7.

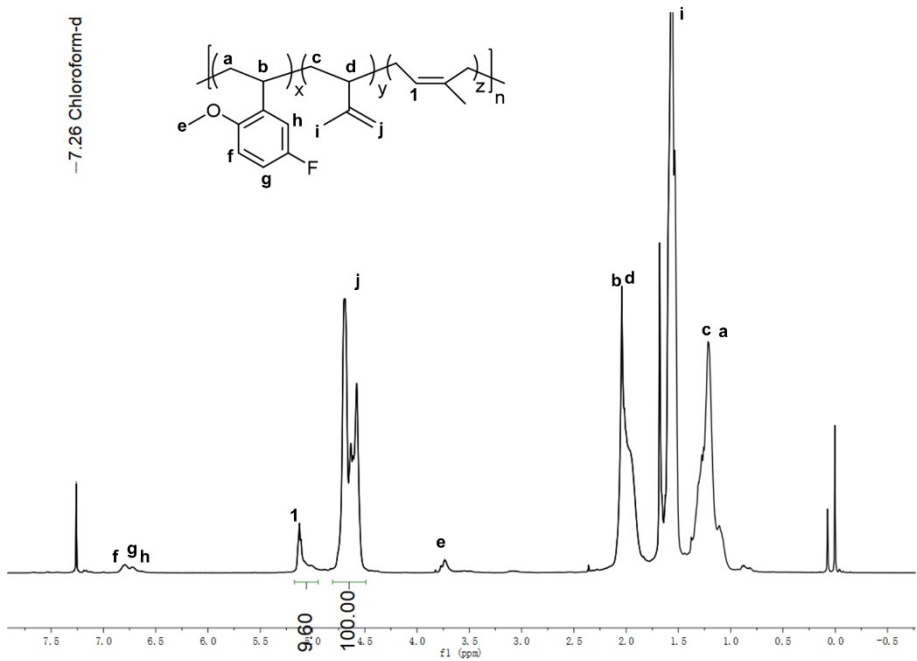


Figure S17. ^1H NMR spectrum of P(2,5-FMOS-*co*-IP) (CDCl_3 , 25°C) in Table 1, entry 8.

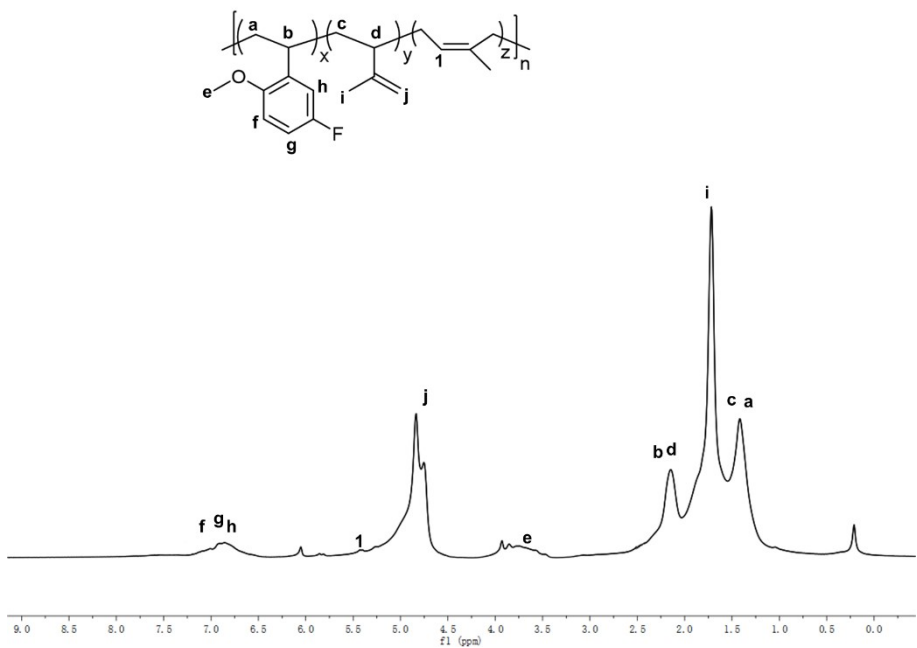


Figure S18. ^1H NMR spectrum of P(2,5-FMOS-*co*-IP) ($\text{C}_2\text{D}_2\text{Cl}_4$, 110°C) in Table 1, entry 11.

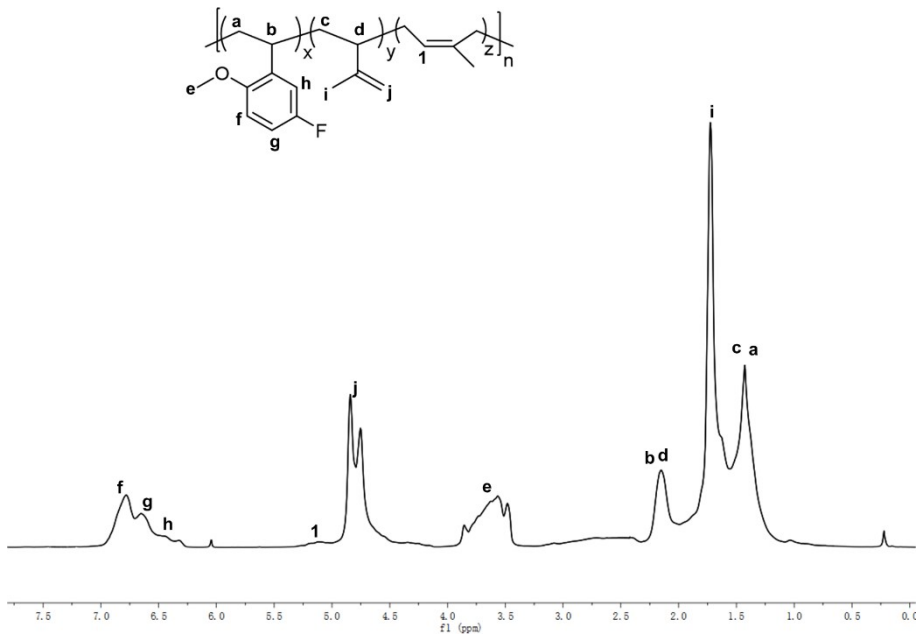


Figure S19. ¹H NMR spectrum of P(2,5-FMOS-*co*-IP) (C₂D₂Cl₄, 110°C) in Table 1, entry 12.

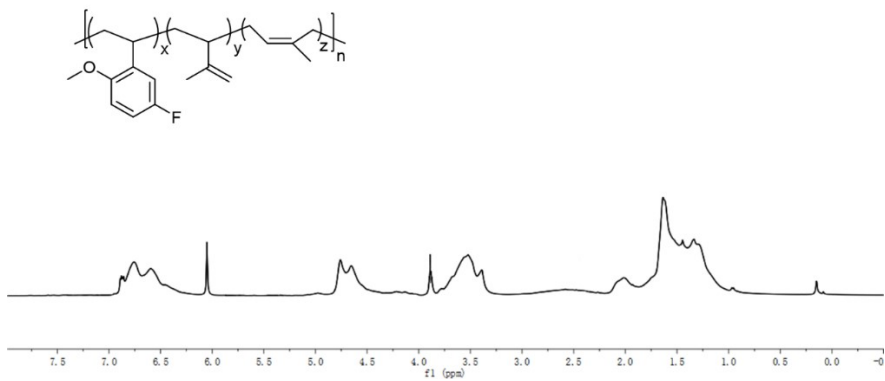


Figure S20. ¹H NMR spectrum of P(2,5-FMOS-*co*-IP) (C₂D₂Cl₄, 110°C) in Table 1, entry 13.

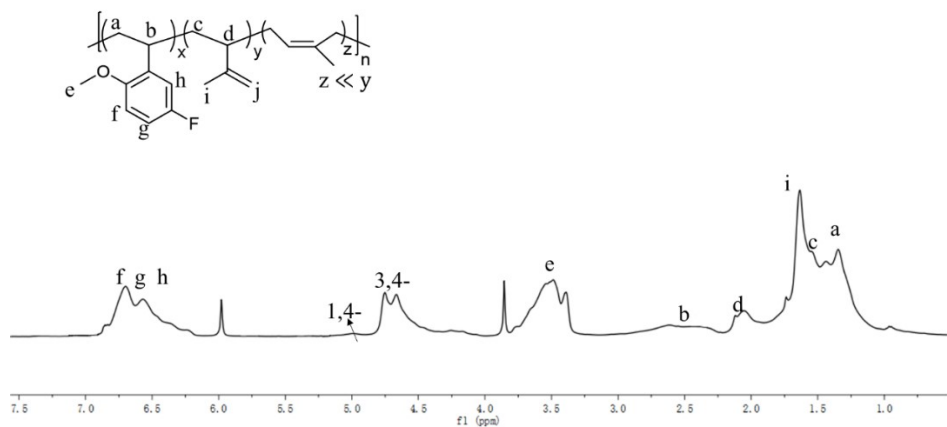


Figure S21. ^1H NMR spectrum of P(2,5-FMOS-*co*-IP) ($\text{C}_2\text{D}_2\text{Cl}_4$, 110°C) in Table 1, entry 14.

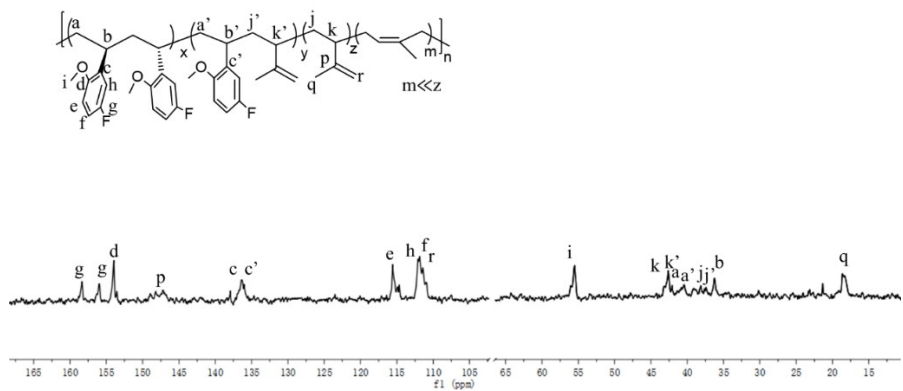


Figure S22. ^{13}C NMR spectrum of P(2,5-FMOS-*co*-IP) ($\text{C}_2\text{D}_2\text{Cl}_4$, 110°C) in Table 1, entry 14.

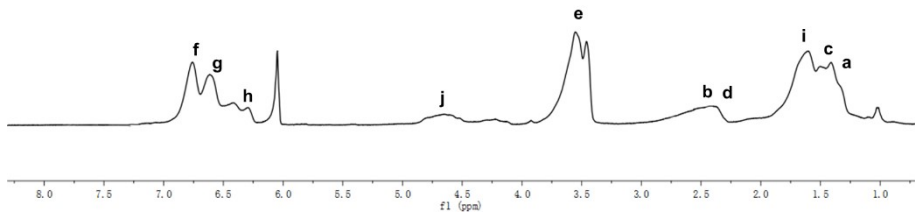
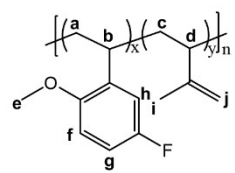


Figure S23. ¹H NMR spectrum of P(2,5-FMOS-*co*-IP) (C₂D₂Cl₄, 110°C) in Table 1, entry 16.

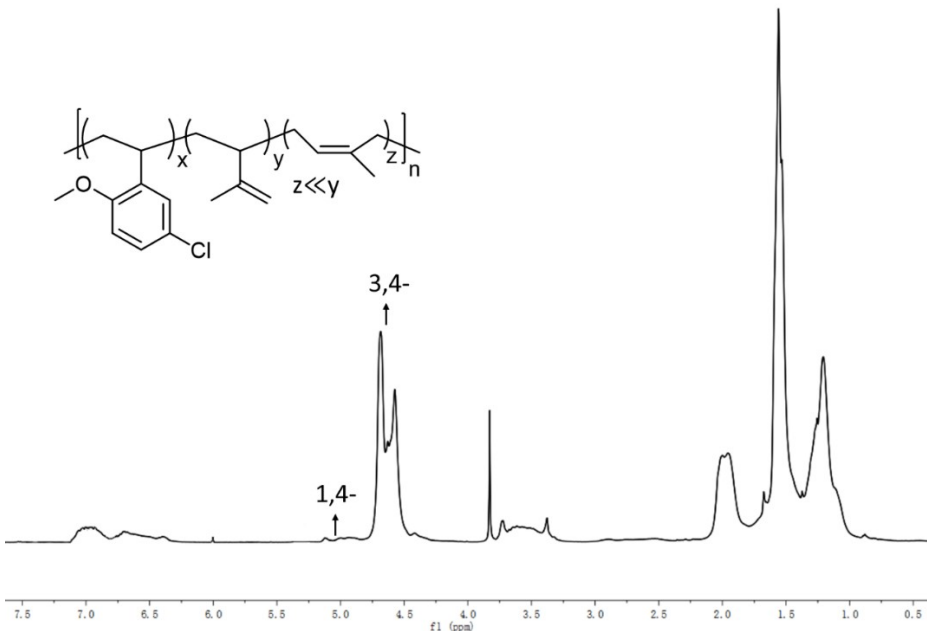
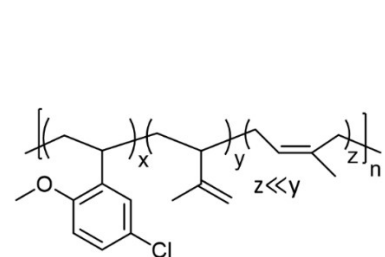


Figure S24. ¹H NMR spectrum of the copolymers P(2,5-ClMOS-*co*-IP) (C₂D₂Cl₄, 110°C) in Table 1, entry 17.

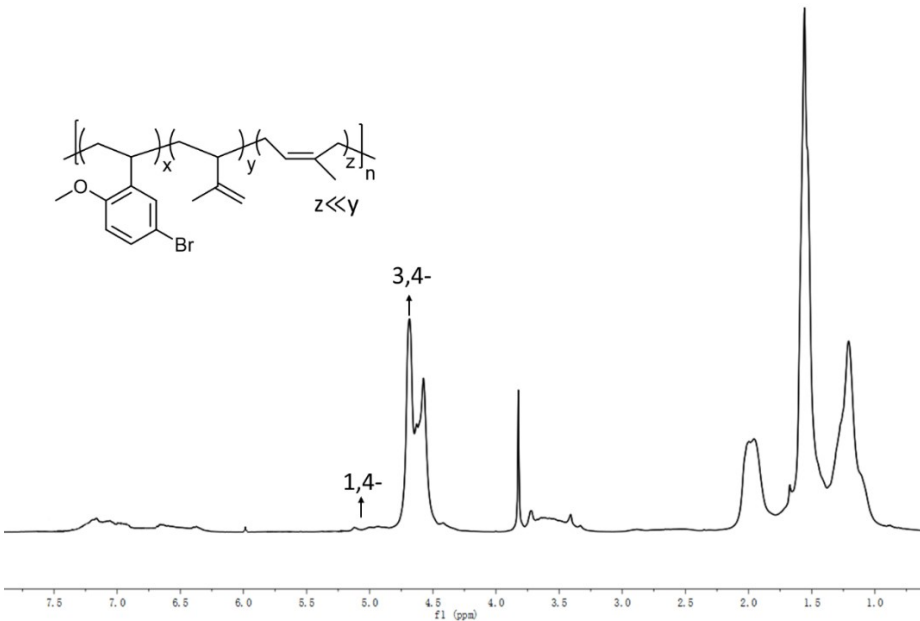


Figure S25. ^1H NMR spectrum of P(2,5-BrMOS-*co*-IP) ($\text{C}_2\text{D}_2\text{Cl}_4$, 110°C) in Table 1, entry 18.

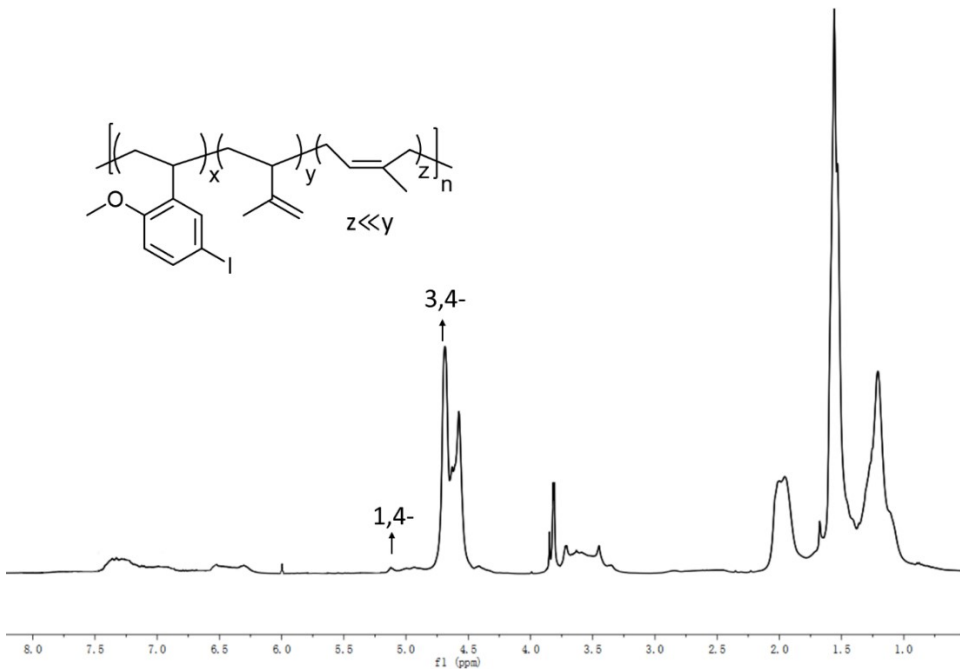


Figure S26. ^1H NMR spectrum of P(2,5-IMOS-*co*-IP) ($\text{C}_2\text{D}_2\text{Cl}_4$, 110°C) in Table 1, entry 19.

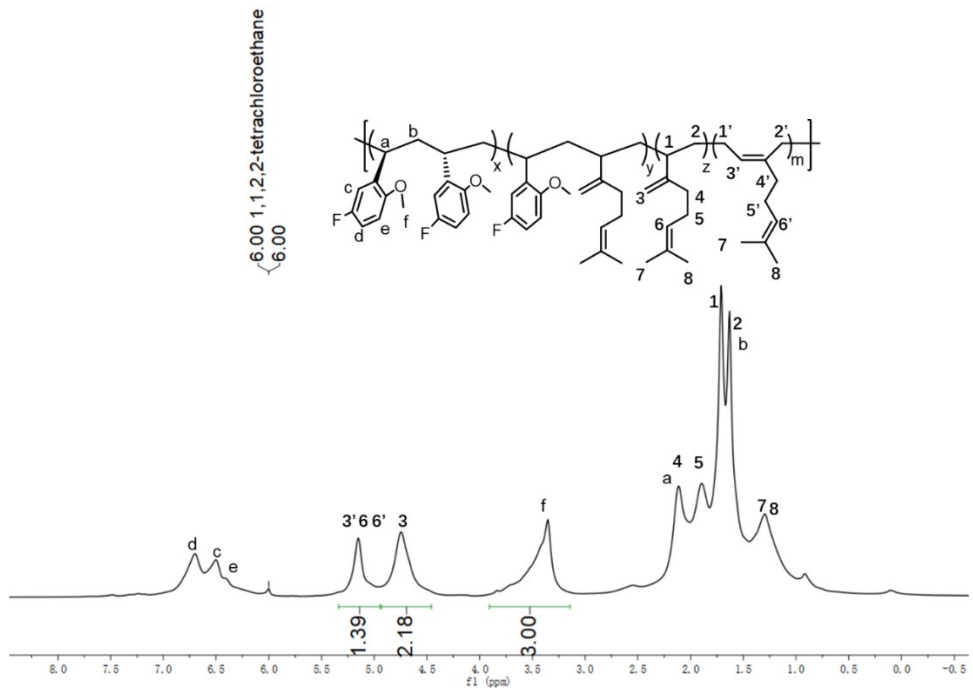


Figure S27. ¹H NMR spectrum of P(2,5-FMOS-*co*-MY) ($\text{C}_2\text{D}_2\text{Cl}_4$, 110°C) in Table 1, entry 20.

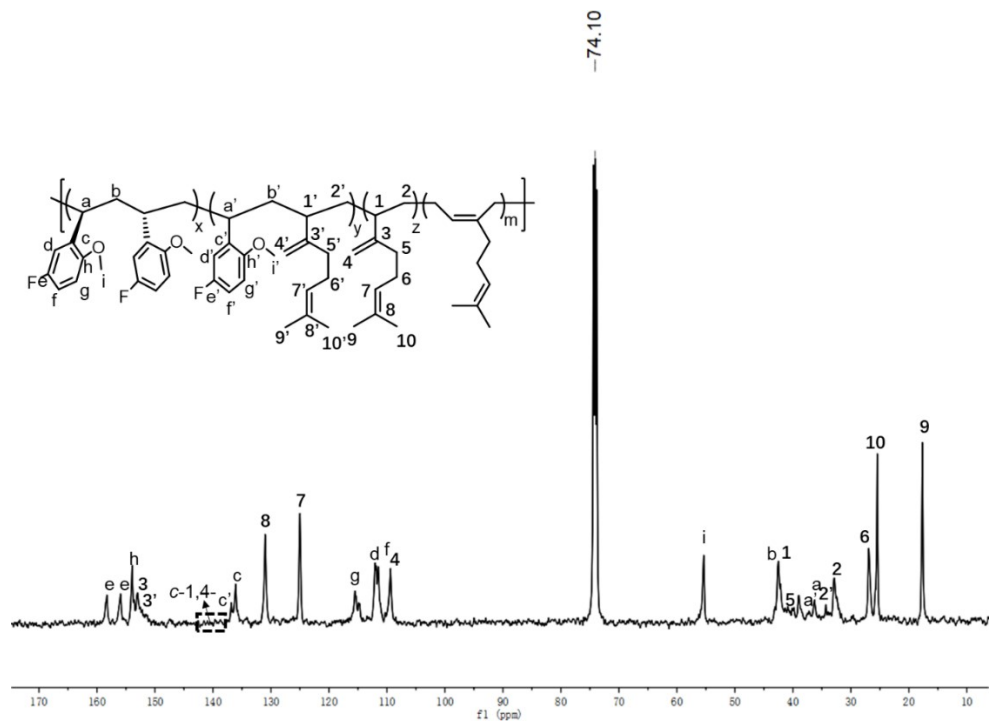


Figure S28. ¹³C NMR spectrum of P(2,5-FMOS-*co*-MY) ($\text{C}_2\text{D}_2\text{Cl}_4$, 110°C) in Table 1, entry 20.

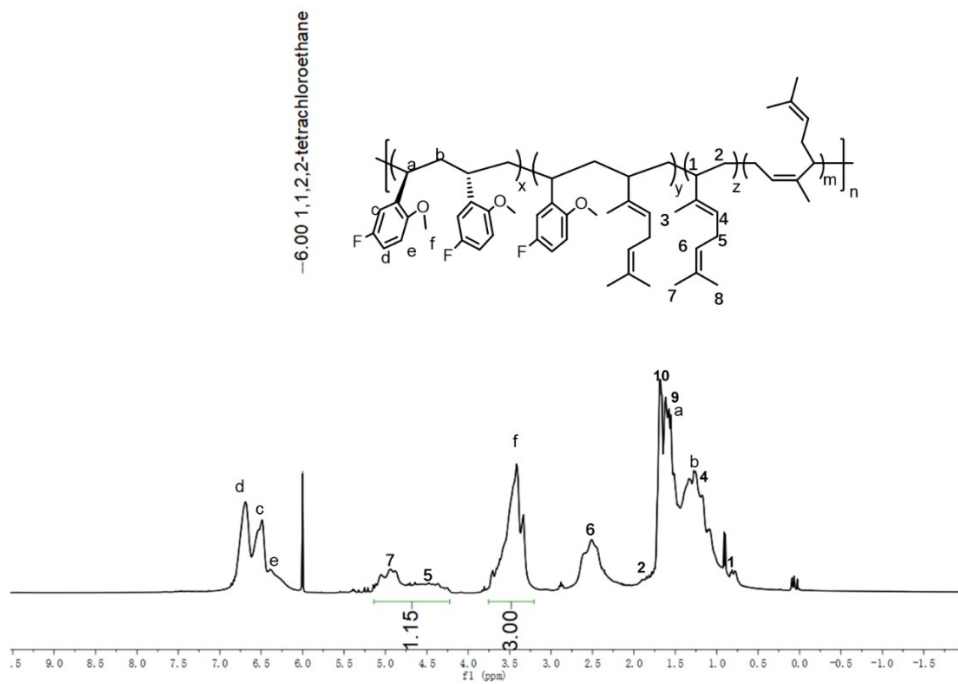


Figure S29. ^1H NMR spectrum of P(2,5-FMOS-*co*-OC) ($\text{C}_2\text{D}_2\text{Cl}_4$, 110°C) in Table 1, entry 21.

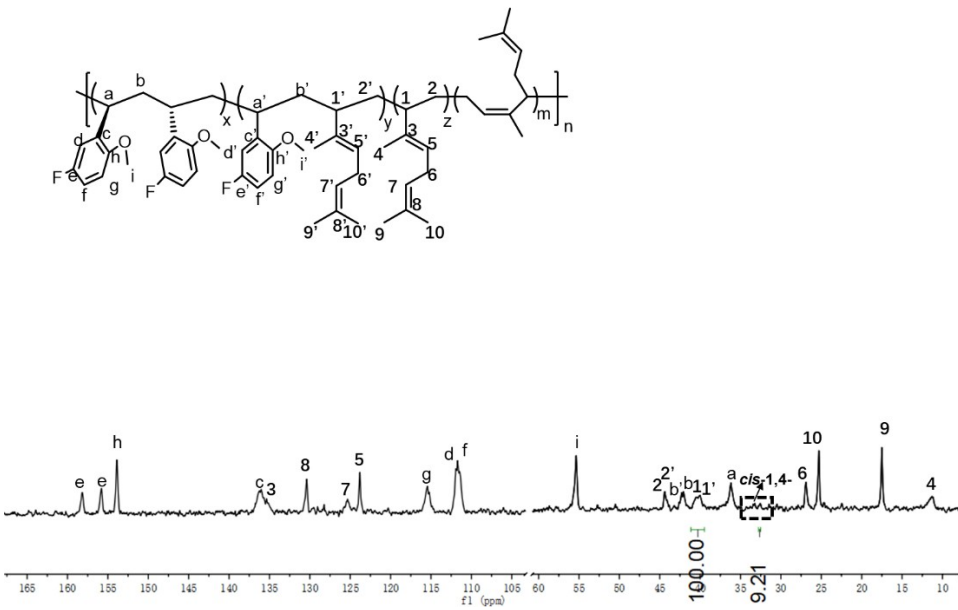
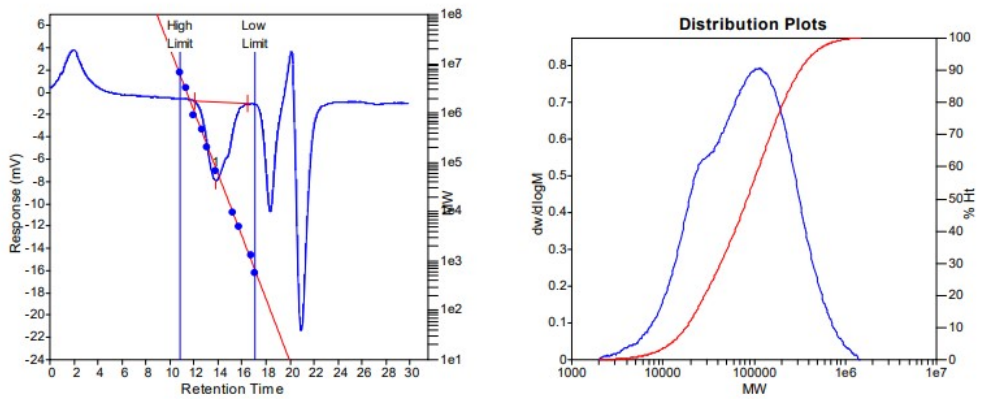


Figure S30. ^{13}C NMR spectrum of P(2,5-FMOS-*co*-OC) ($\text{C}_2\text{D}_2\text{Cl}_4$, 110°C) in Table 1, entry 21.

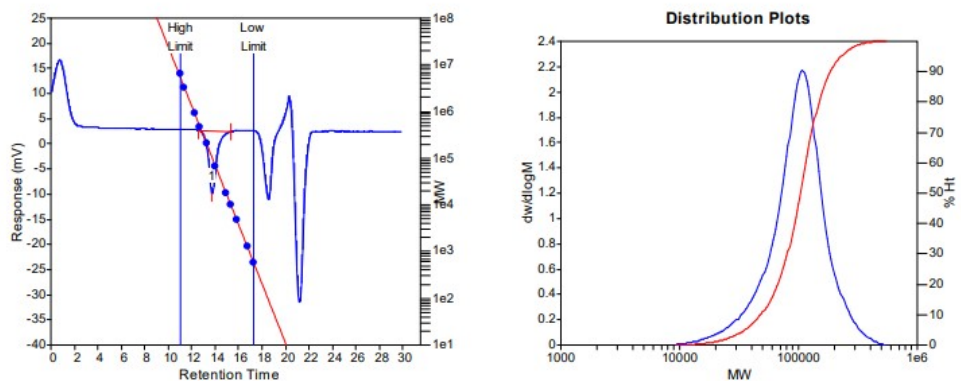
GPC curve of polymers P(CDs-*co*-PO)s



MW Averages

Peak No	M _p	M _n	M _w	M _z	M _{z+1}	M _v	PD
1	113914	40852	134573	309475	515470	111166	3.29416

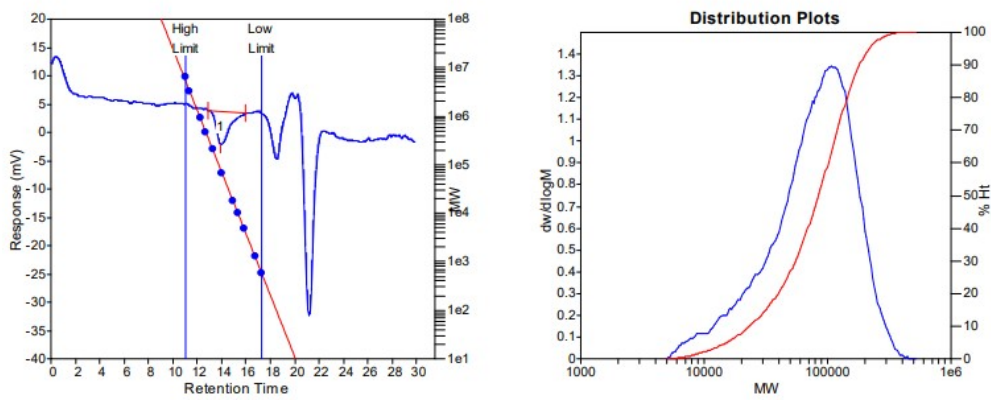
Figure S31. GPC curve of PIP in Table 1, entry 1.



MW Averages

Peak No	M _p	M _n	M _w	M _z	M _{z+1}	M _v	PD
1	107189	81885	111790	143933	182753	106993	1.36521

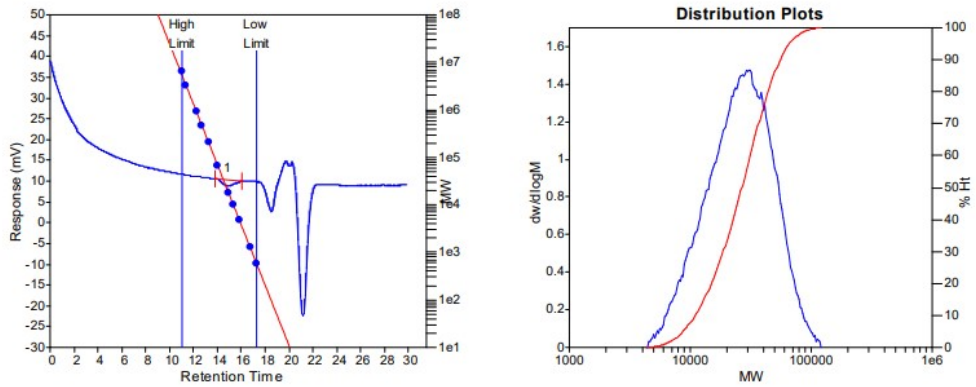
Figure S32. GPC curve of P(*o*MOS-*co*-IP) in Table 1, entry 2.



MW Averages

Peak No	Mp	Mn	Mw	Mz	Mz+1	Mv	PD
1	106665	49913	94692	136970	174505	86841	1.89714

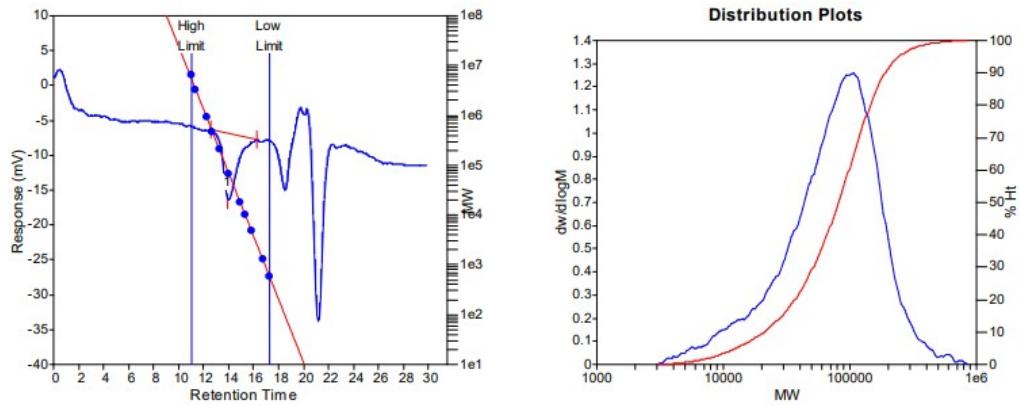
Figure S33. GPC curve of P(*m*MOS-*co*-IP) in Table 1, entry 3.



MW Averages

Peak No	Mp	Mn	Mw	Mz	Mz+1	Mv	PD
1	30484	20865	30181	40915	51700	28324	1.44649

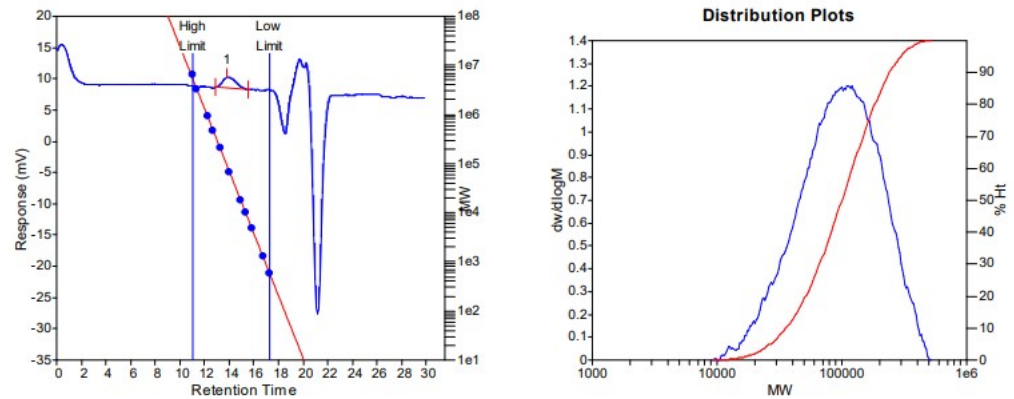
Figure S34. GPC curve of P(*m*MOS-*co*-IP) in Table 1, entry 4.



MW Averages

Peak No	M _p	M _n	M _w	M _z	M _{z+1}	M _v	PD
1	106665	44010	97987	167017	265409	87562	2.22647

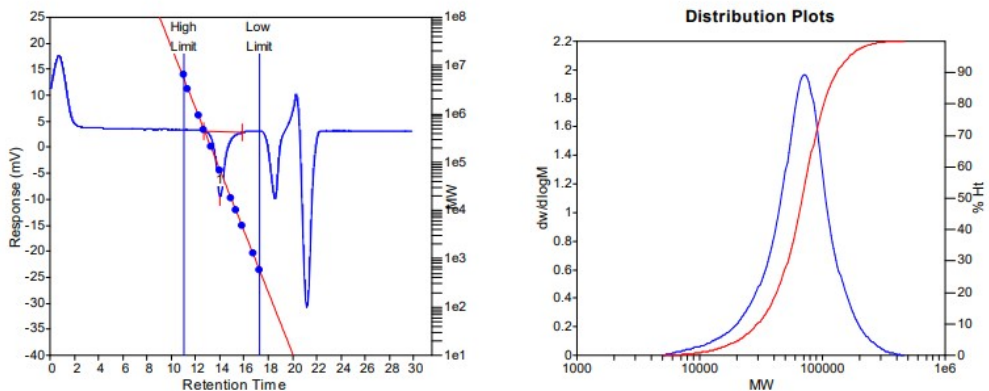
Figure S35. GPC curve of P(*p*MOS-*co*-IP) in Table 1, entry 5.



MW Averages

Peak No	M _p	M _n	M _w	M _z	M _{z+1}	M _v	PD
1	109370	71939	120715	178864	233906	110801	1.67802

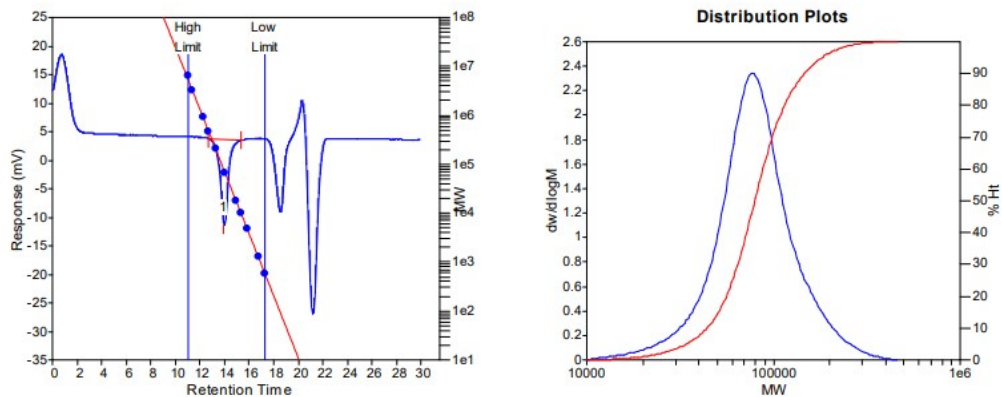
Figure S36. GPC curve of P(*p*MOS-*co*-IP) in Table 1, entry 6.



MW Averages

Peak No	M _p	M _n	M _w	M _z	M _{z+1}	M _v	PD
1	72573	51770	75889	103051	137808	71974	1.46589

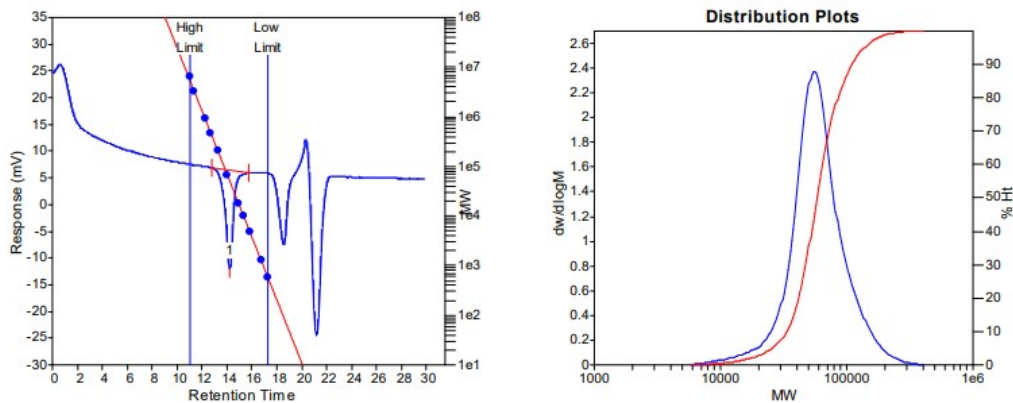
Figure S37. GPC curve of P(2,5-FMOS-*co*-IP) in Table 1, entry 7.



MW Averages

Peak No	M _p	M _n	M _w	M _z	M _{z+1}	M _v	PD
1	78079	68822	88280	112726	145525	84857	1.28273

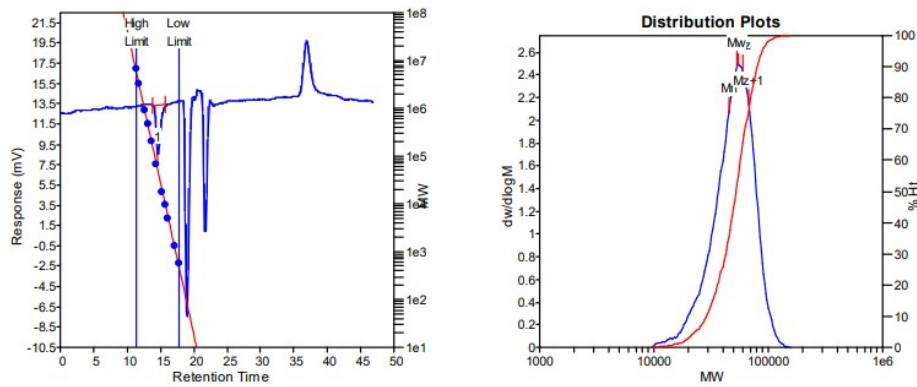
Figure S38. GPC curve of P(2,5-FMOS-*co*-IP) in Table 1, entry 8.



MW Averages

Peak No	M _p	M _n	M _w	M _z	M _{z+1}	M _v	PD
1	55505	50420	65795	85984	115484	63075	1.30494

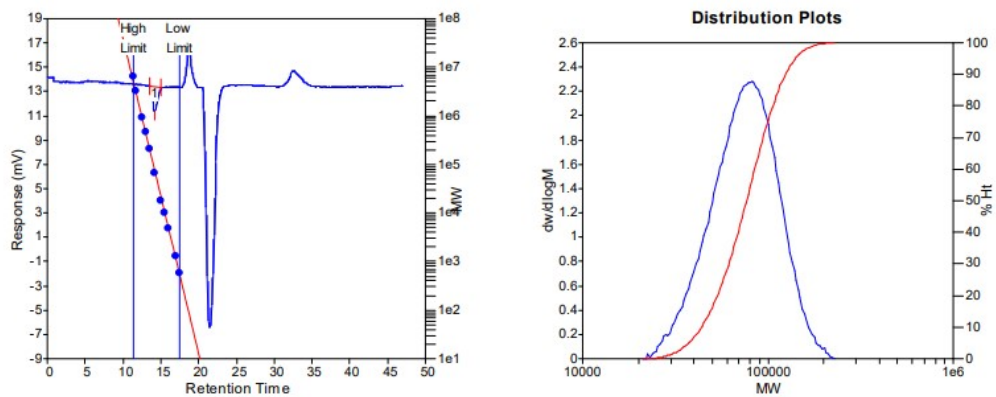
Figure S39. GPC curve of P(2,5-FMOS-*co*-IP) in Table 1, entry 9.



MW Averages

Peak No	M _p	M _n	M _w	M _z	M _{z+1}	M _v	PD
1	54872	44875	53108	60535	67358	51855	1.18347

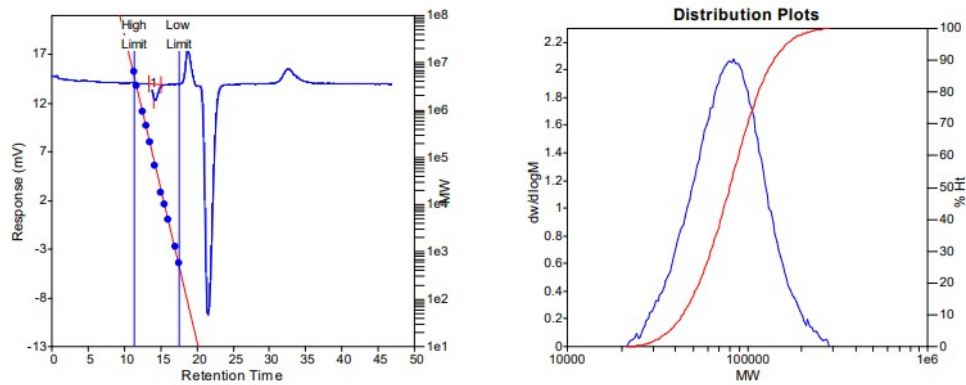
Figure S40. GPC curve of P(2,5-FMOS-*co*-IP) in Table 1, entry 10.



MW Averages

Peak No	M _p	M _n	M _w	M _z	M _{z+1}	M _v	PD
1	82197	68434	80176	92542	105027	78206	1.17158

Figure S41. GPC curve of P(2,5-FMOS-*co*-IP) in Table 1, entry 11.



MW Averages

Peak No	M _p	M _n	M _w	M _z	M _{z+1}	M _v	PD
1	84267	70594	86136	104328	124651	83393	1.22016

Figure S42. GPC curve of P(2,5-FMOS-*co*-IP) in Table 1, entry 12.

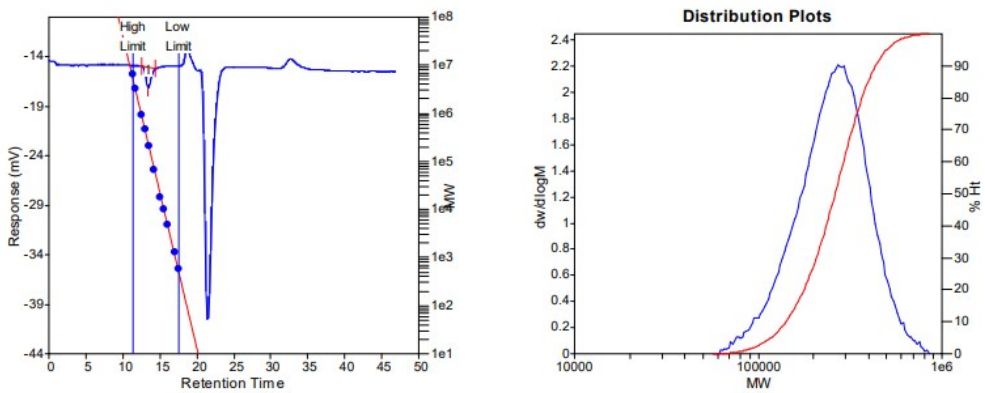


Figure S43. GPC curve of P(2,5-FMOS-*co*-IP) in Table 1, entry 13.

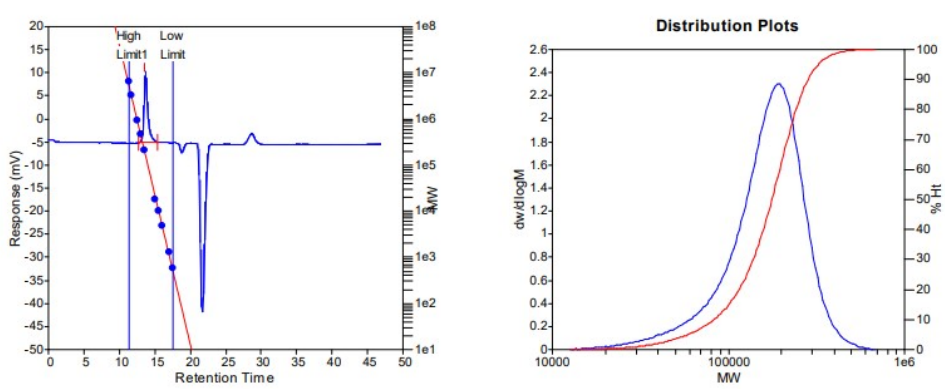
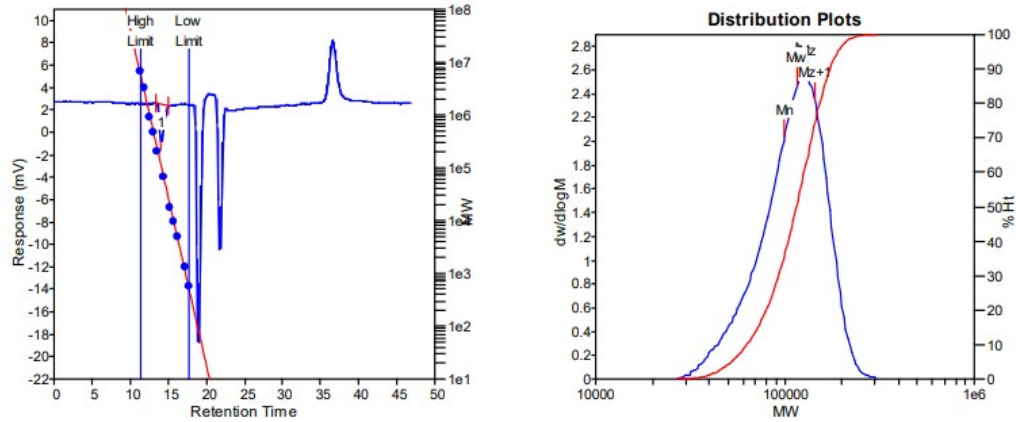


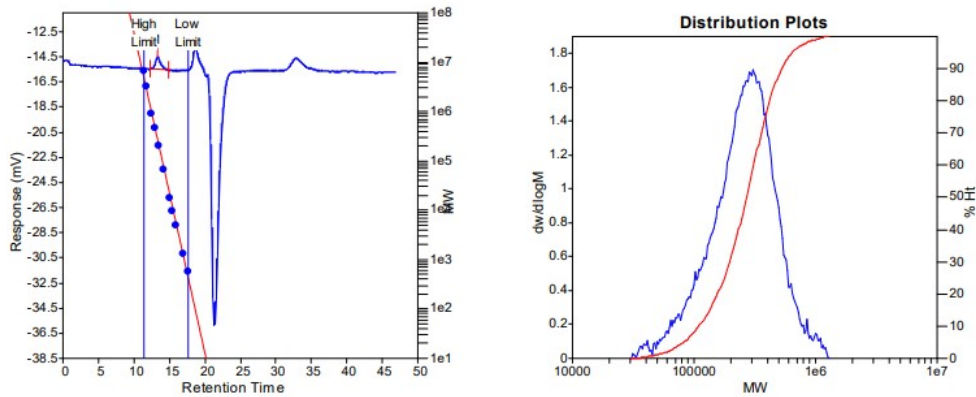
Figure S44. GPC curve of P(2,5-FMOS-*co*-IP) in Table 1, entry 14.



MW Averages

Peak No	Mp	Mn	Mw	Mz	Mz+1	Mv	PD
1	125937	99611	116039	131041	144496	113495	1.16492

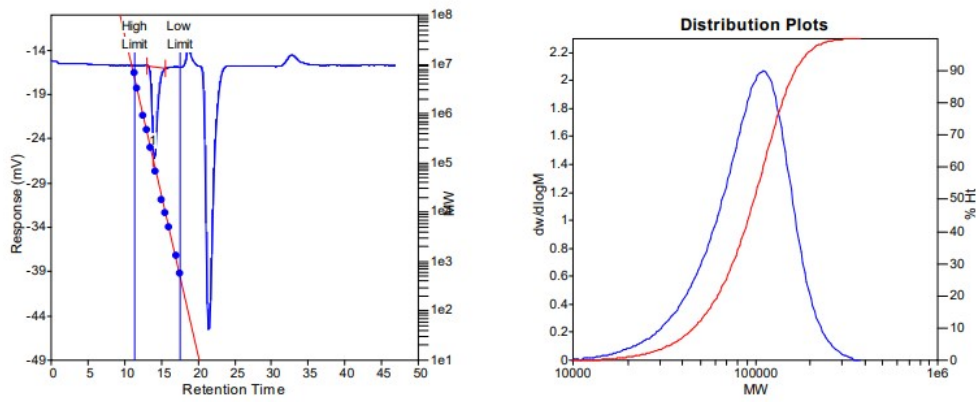
Figure S45. GPC curve of P(2,5-FMOS-*co*-IP) in Table 1, entry 15.



MW Averages

Peak No	Mp	Mn	Mw	Mz	Mz+1	Mv	PD
1	307195	203978	299453	407573	530947	283406	1.46807

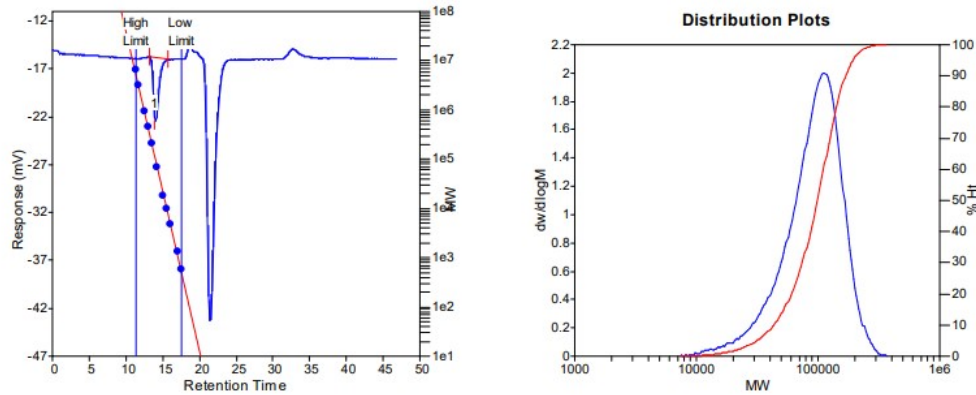
Figure S46. GPC curve of P(2,5-FMOS-*co*-IP) in Table 1, entry 16.



MW Averages

Peak No	M _p	M _n	M _w	M _z	M _{z+1}	M _v	PD
1	110788	77869	102142	124244	145282	98484	1.31172

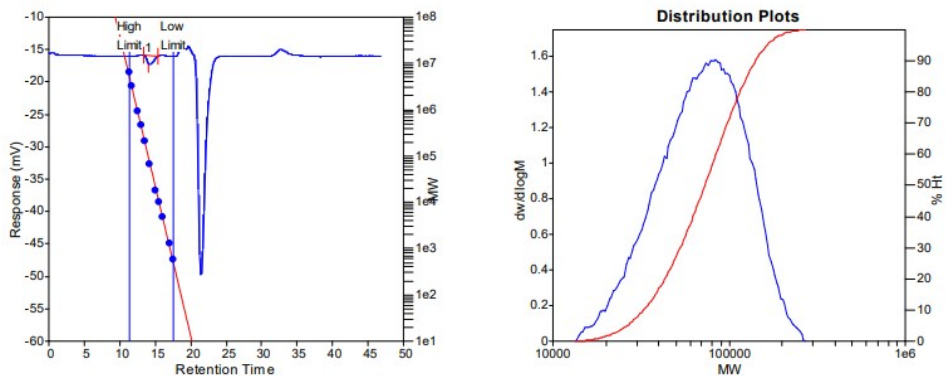
Figure S47. GPC curve of P(2,5-ClMOS-*co*-IP) in Table 1, entry 17.



MW Averages

Peak No	M _p	M _n	M _w	M _z	M _{z+1}	M _v	PD
1	113578	74551	102224	125725	146973	98244	1.3712

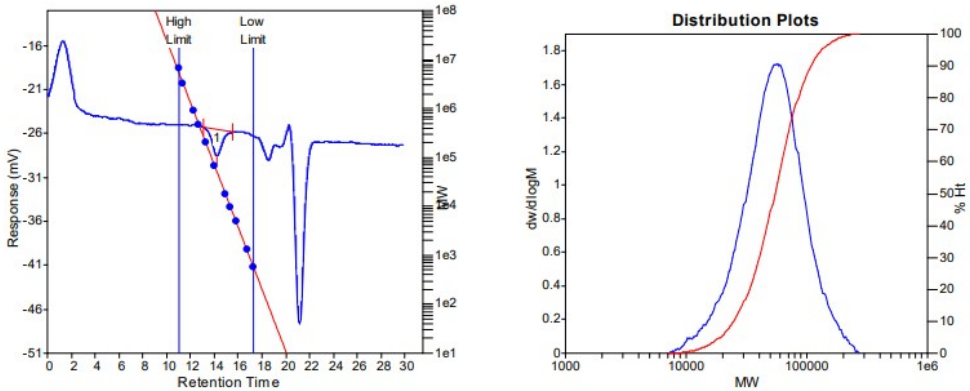
Figure S48. GPC curve of P(2,5-BrMOS-*co*-IP) in Table 1, entry 18.



MW Averages

Peak No	Mp	Mn	Mw	Mz	Mz+1	Mv	PD
1	84267	58997	79994	102618	124188	76425	1.3559

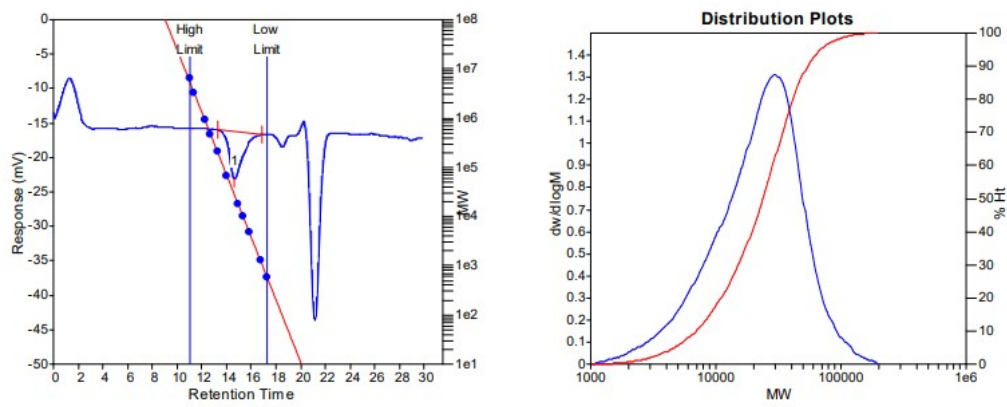
Figure S49. GPC curve of P(2,5-IMOS-*co*-IP) in Table 1, entry 19.



MW Averages

Peak No	Mp	Mn	Mw	Mz	Mz+1	Mv	PD
1	56875	43781	61177	82203	106529	58118	1.39734

Figure S50. GPC curve of P(2,5-FMOS-*co*-MY) in Table 1, entry 20.



MW Averages

Peak No	Mp	Mn	Mw	Mz	Mz+1	Mv	PD
1	30178	14363	28087	44752	65112	25740	1.95551

Figure S51. GPC curve of P(2,5-FMOS-*co*-OC) in Table 1, entry 21.

DSC curve of polymers P(CDs-*co*-PO)s

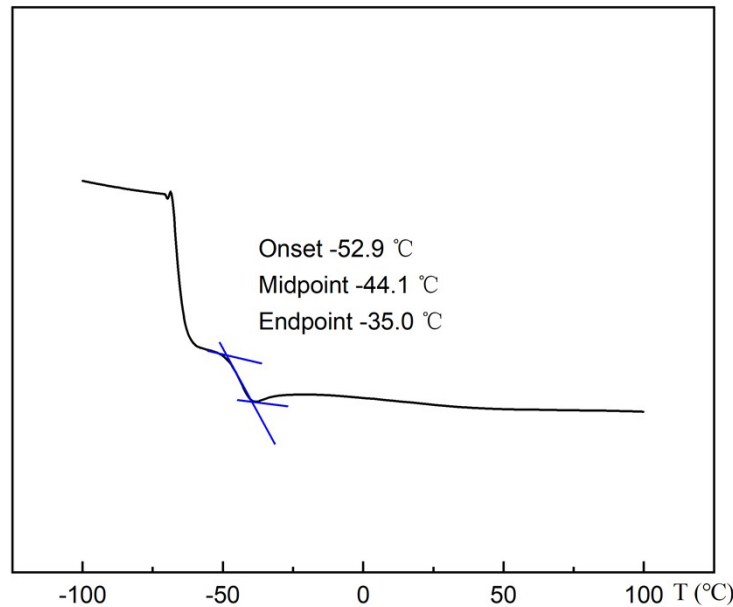


Figure S52. DSC curve of PIP in Table 1, entry 1.

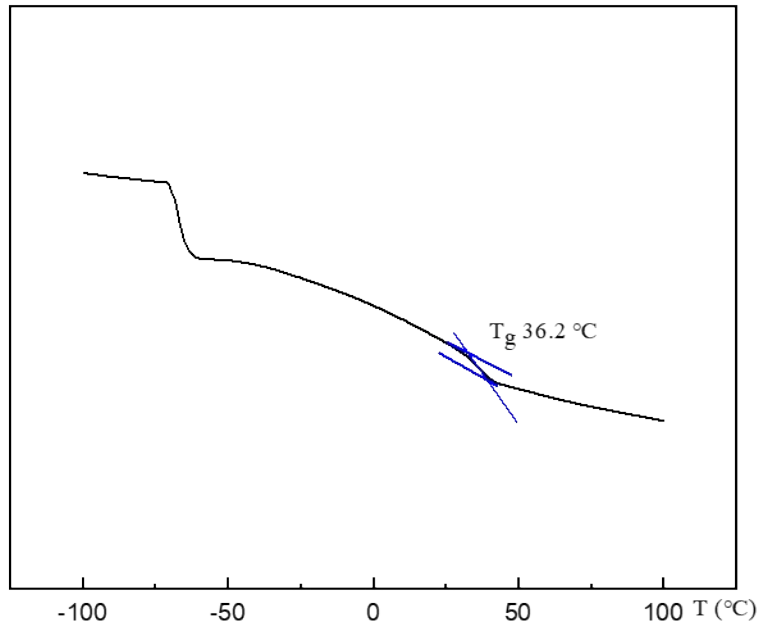


Figure S53. DSC curve of P(*o*MOS-*co*-IP) in Table 1, entry 2.

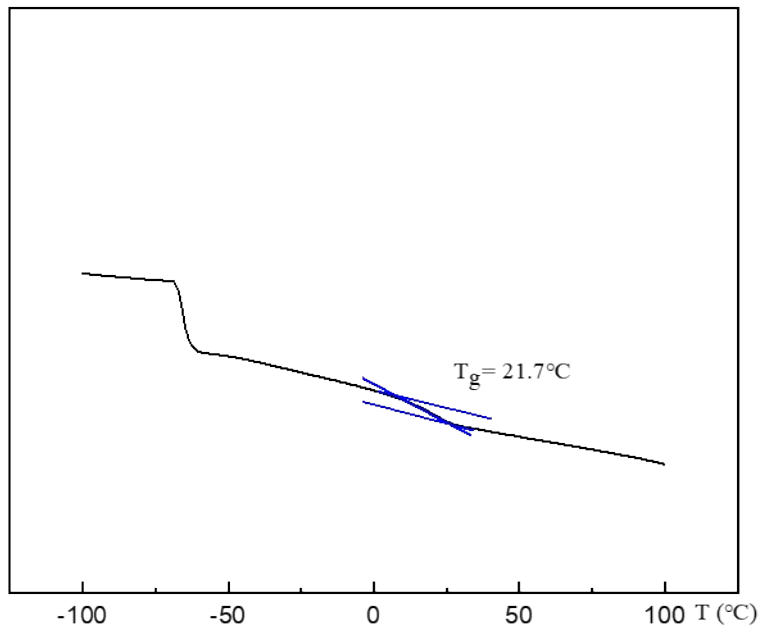


Figure S54. DSC curve of P(*m*MOS-*co*-IP) in Table 1, entry 3.

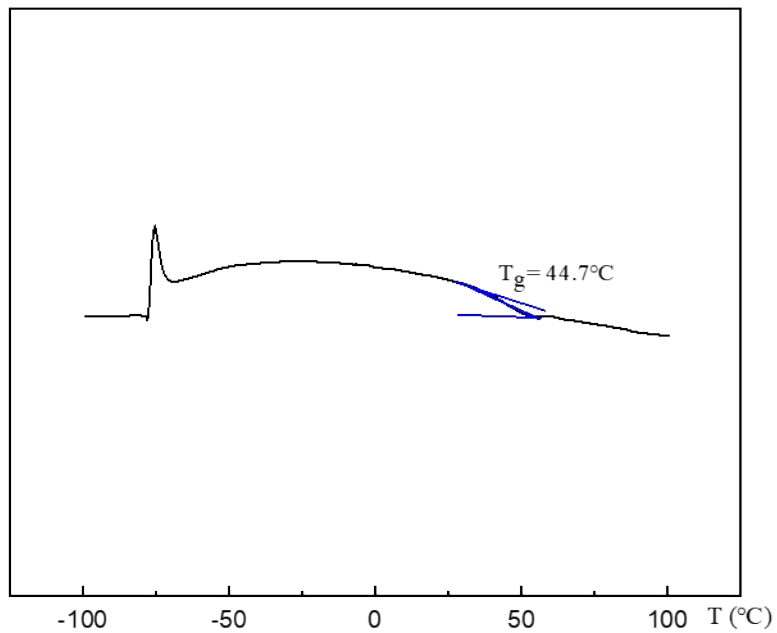


Figure S55. DSC curve of P(*m*MOS-*co*-IP) in Table 1, entry 4.

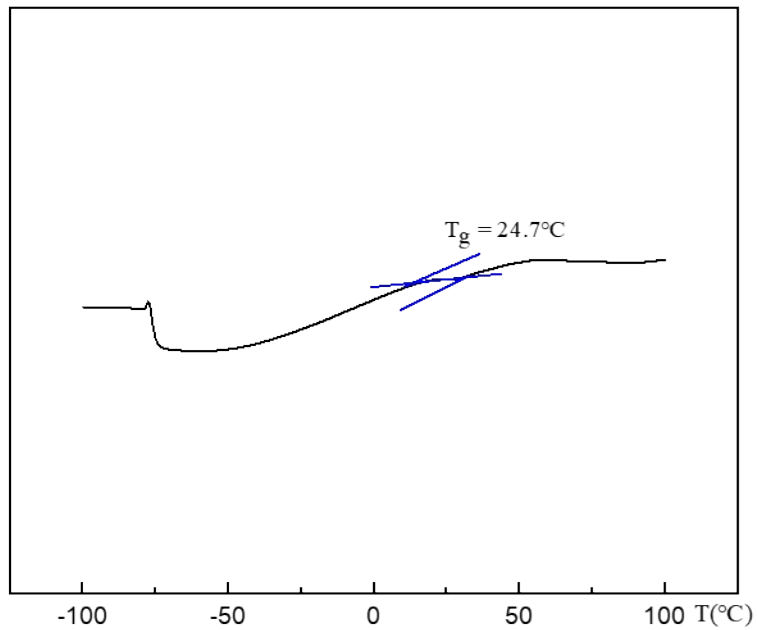


Figure S56. DSC curve of P(*p*MOS-*co*-IP) in Table 1, entry 5.

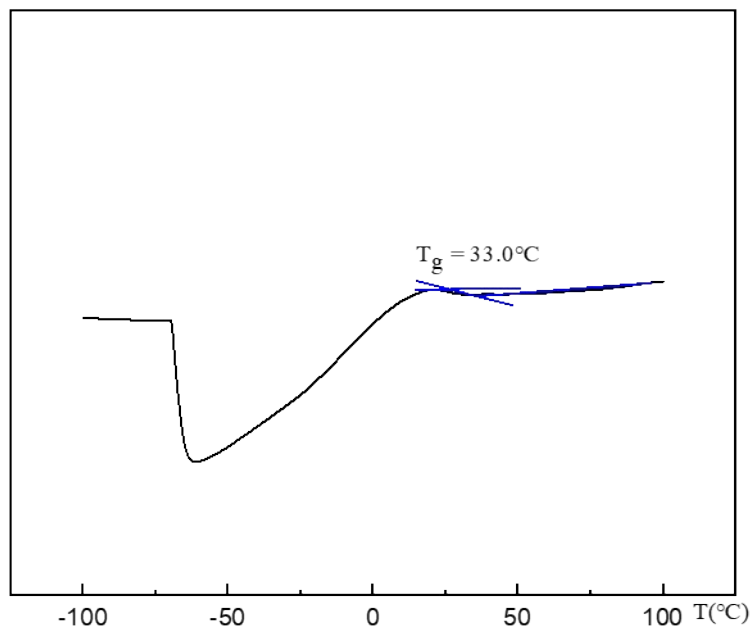


Figure S57. DSC curve of P(*p*MOS-*co*-IP) in Table 1, entry 6.

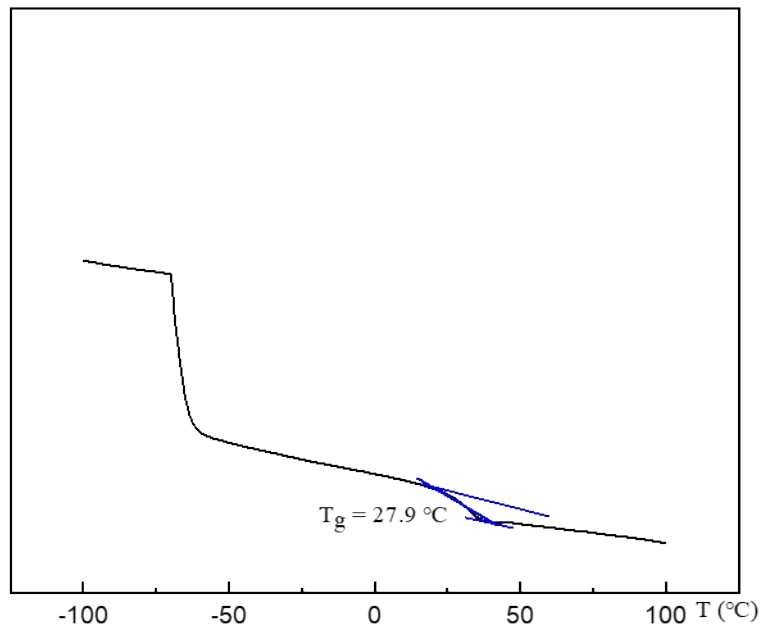


Figure S58. DSC curve of P(2,5-FMOS-*co*-IP) in Table 1, entry 8.

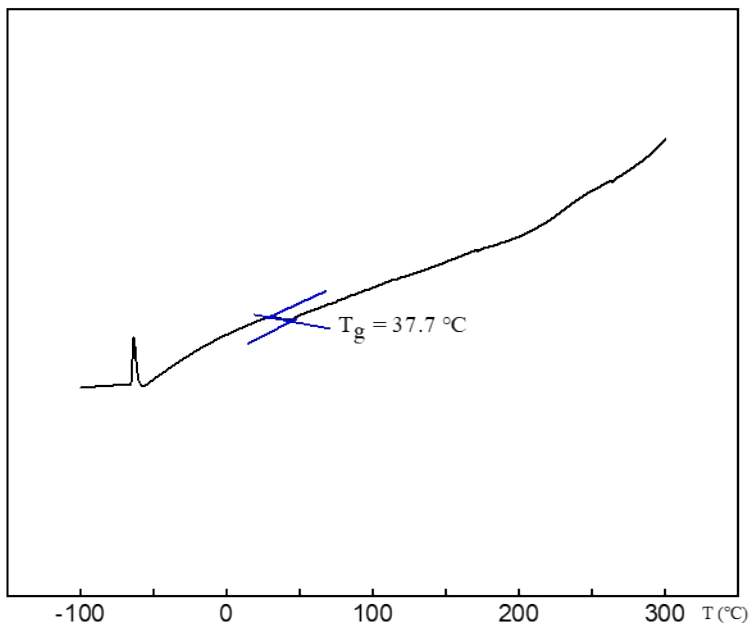


Figure S59. DSC curve of P(2,5-FMOS-*co*-IP) in Table 1, entry 10.

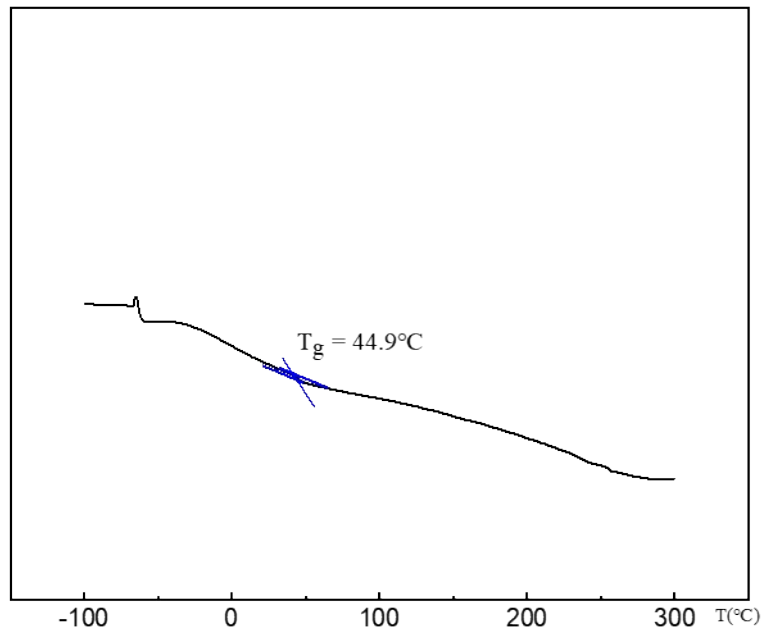


Figure S60. DSC curve of P(2,5-FMOS-*co*-IP) in Table 1, entry 11.

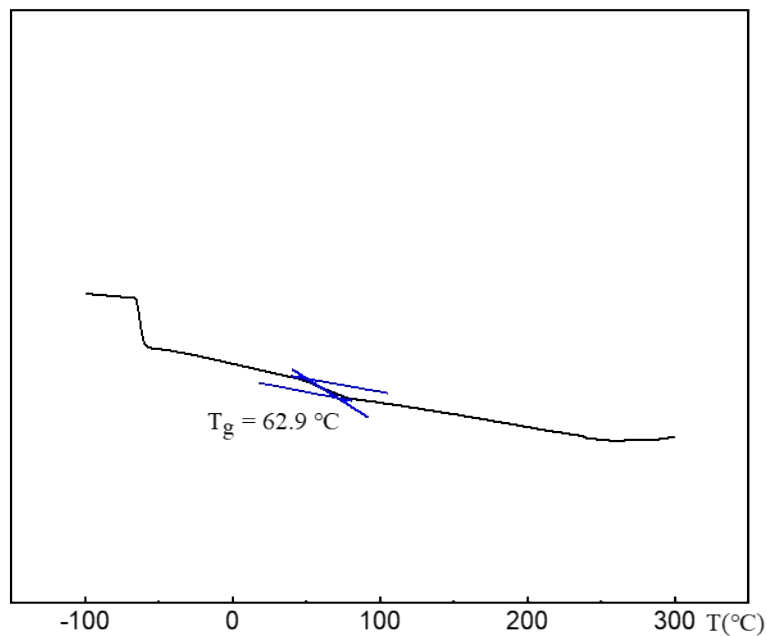


Figure S61. DSC curve of P(2,5-FMOS-*co*-IP) in Table 1, entry 13.

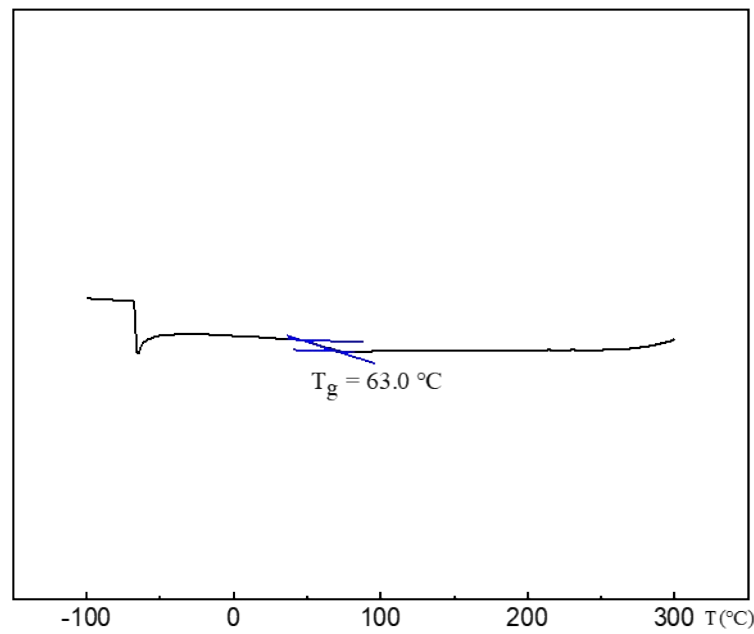


Figure S62. DSC curve of P(2,5-FMOS-*co*-IP) in Table 1, entry 14.

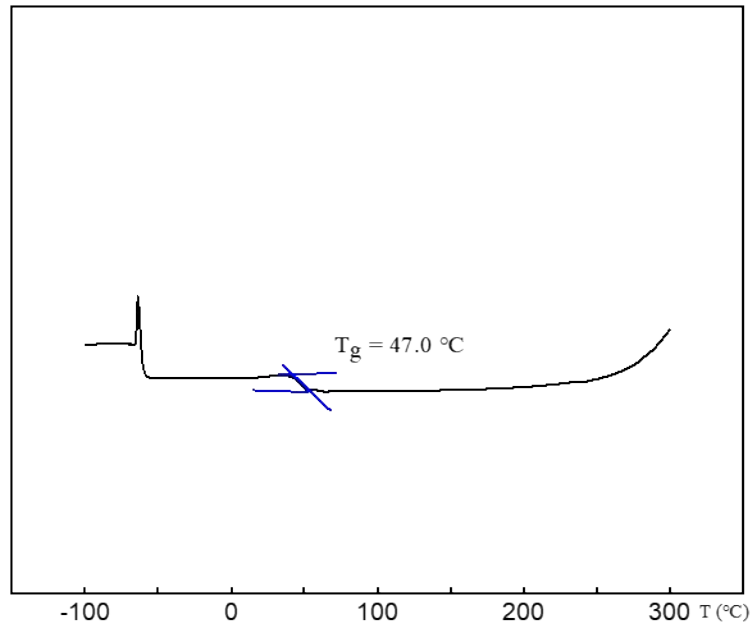


Figure S63. DSC curve of P(2,5-ClMOS-*co*-IP) in Table 1, entry 17.

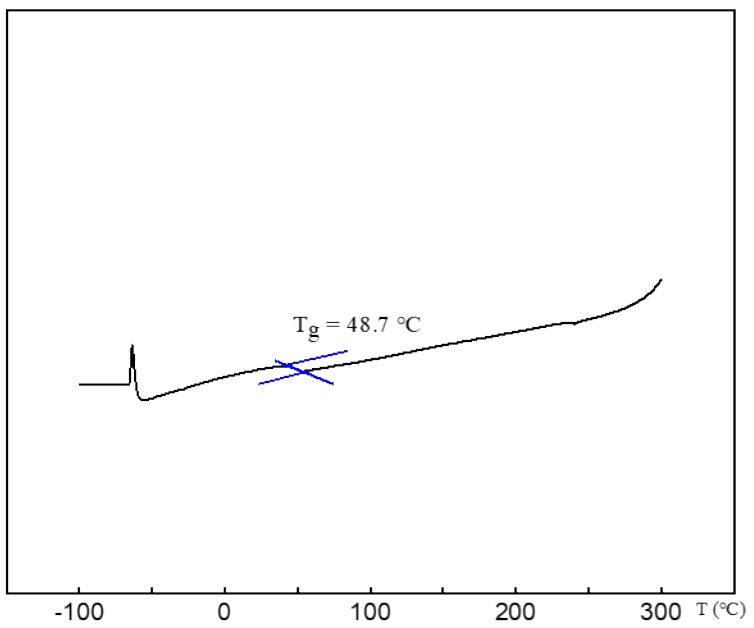


Figure S64. DSC curve of P(2,5-BrMOS-*co*-IP) in Table 1, entry 18.

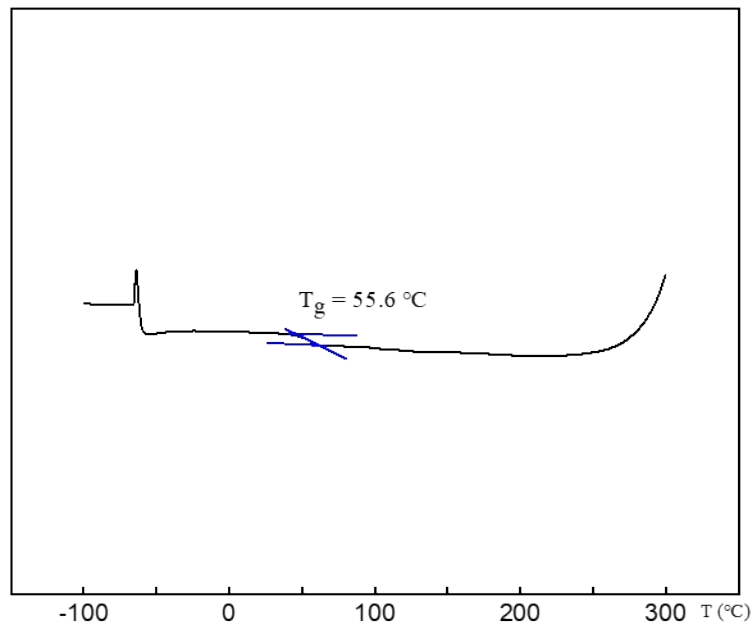


Figure S65. DSC curve of P(2,5-IMOS-*co*-IP) in Table 1, entry 19.

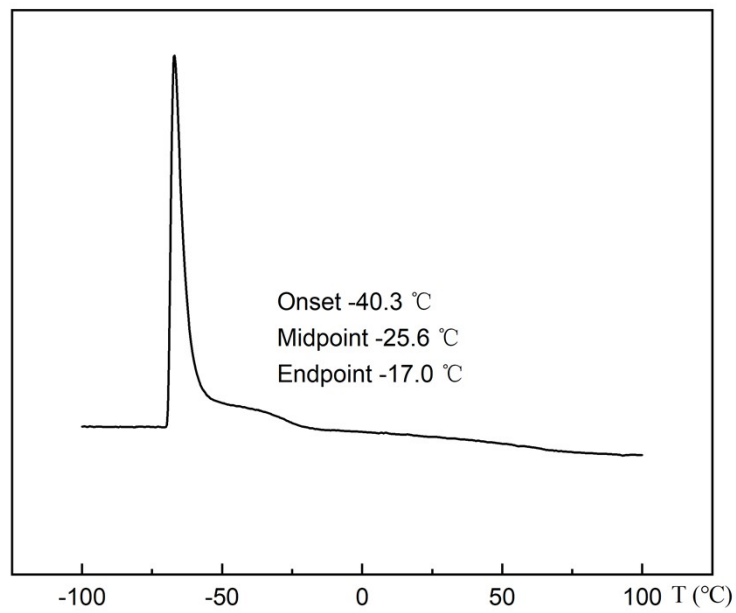


Figure S66. DSC curve of P(2,5-FMOS-*co*-MY) in Table 1, entry 20.

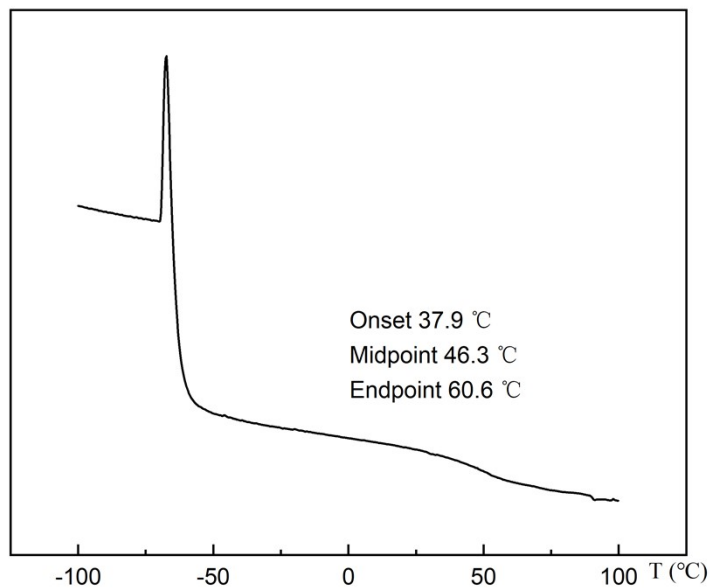


Figure S67. DSC curve of P(2,5-FMOS-*co*-OC) in Table 1, entry 21.

Rheological measurements

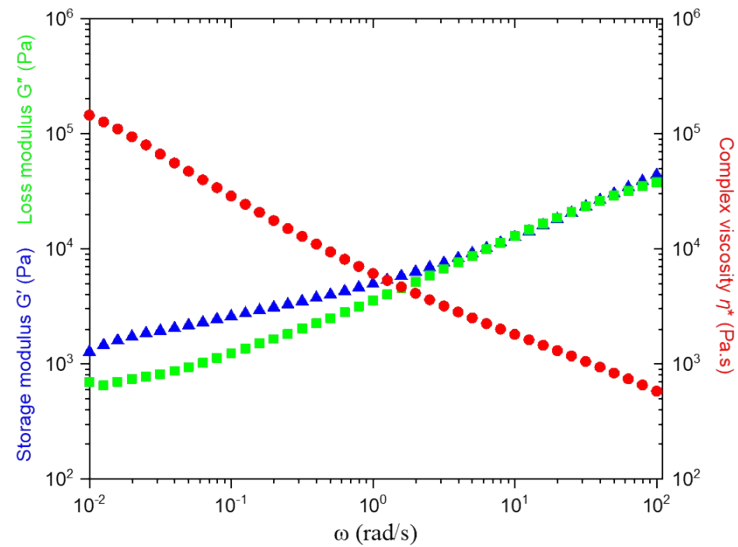


Figure S68. Complex viscosity (η^*), storage modulus (G') and loss modulus (G'') as a function of frequency of copolymers P(2,5-FMOS-*co*-IP) with 84 mol % IP contents ($\gamma = 10\%$, $T = 180\text{ }^\circ\text{C}$) (Table 1, entry 11).

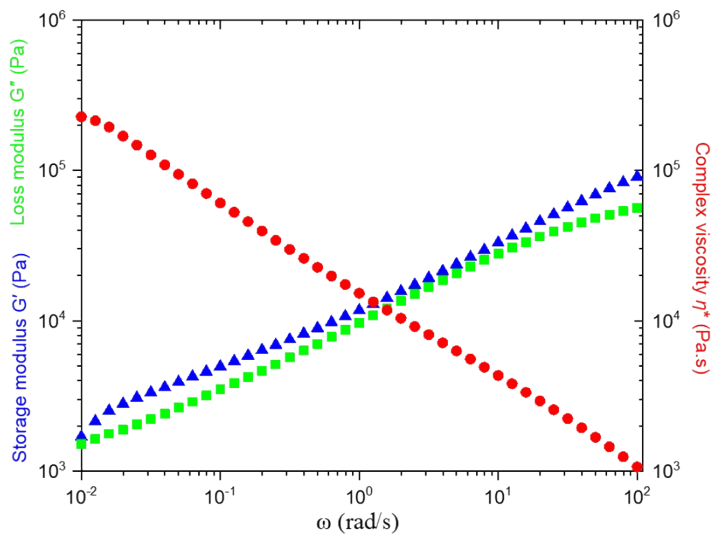


Figure S69. Complex viscosity (η^*), storage modulus (G') and loss modulus (G'') as a function of frequency of copolymers P(2,5-FMOS-*co*-IP) with 71 mol % IP contents ($\gamma = 10\%$, $T = 180\text{ }^\circ\text{C}$) (Table 1, entry 12).

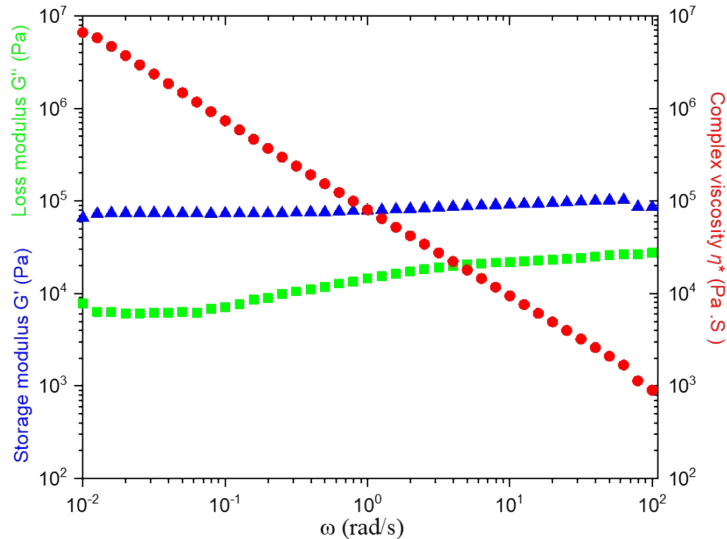
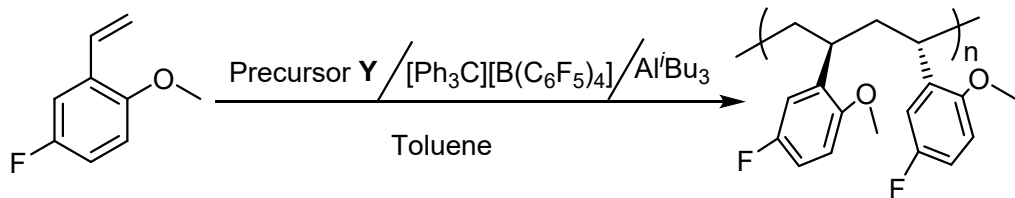


Figure S70. Complex viscosity (η^*), storage modulus (G') and loss modulus (G'') as a function of frequency of copolymers P(2,5-FMOS-*co*-IP) with 29 mol % IP contents ($\gamma = 10\%$, $T = 180\text{ }^\circ\text{C}$) (Table 1, entry 16).

Table S1. polymerization of 2,5-FMOS by the complex $\text{Y}/\text{Al}^{\text{i}}\text{Bu}_3/[\text{Ph}_3\text{C}][\text{B}(\text{C}_6\text{F}_5)_4]$ ternary system^a



Entry	Mon./Cat.	Time (min)	Conv. (%)	<i>rrrr</i> (%) ^b	$M_n(10^4)^c$	M_w/M_n^c	$T_g/T_m({}^\circ\text{C})^e$
1	200:1	20	94	99	3.58	1.31	92.3/—
2	600:1	20	75	99	7.12	1.28	94.2/—

^aGeneral conditions: 10 μmol Cat. Y, 10 μmol [Ph₃C][B(C₆F₅)₄], 100 μmol AlBu₃, Solvent: 1.5 mL Tol., Temperature: 20°C. ^bDetermined by ¹³C NMR spectroscopy. ^cDetermined by GPC in 1,2,4-trichlorobenzene at 150°C against a polystyrene standard. ^dDetermined by DSC.

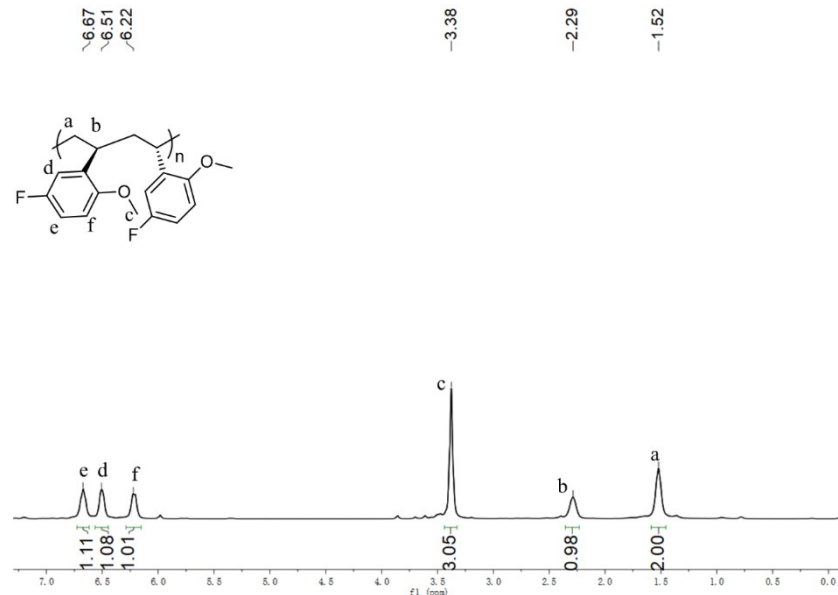


Figure S71. ¹H NMR spectrum of syndiotactic P(2,5-FMOS) (C₂D₂Cl₄, 110°C) in Table S1, entry 1.

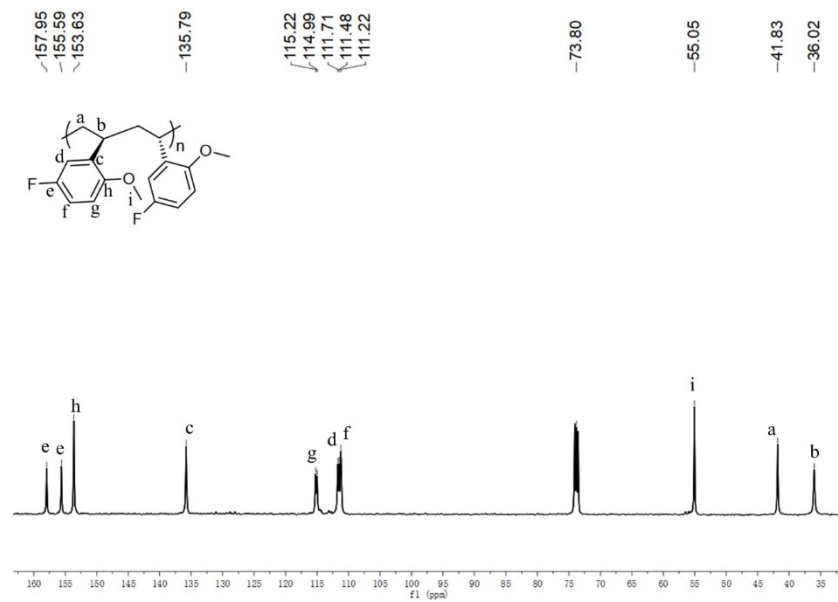


Figure S72. ¹³C NMR spectrum of syndiotactic P(2,5-FMOS) (C₂D₂Cl₄, 110°C) in Table S1, entry 1.

Copolymerization reactivity ratios and intermittent experiment

Reactivity ratios

Table S2: reactivity ratios experiment of copolymerization of IP and 2,5-FMOS^a

2,5-FMOS (mmol)	IP(mmol)	2,5-FMOS Cont. (mol %) ^b	IP Cont. (mol %) ^b	F	f	X	Y
1	5	19.6	80.4	0.2	0.243	0.165	-0.623
2	4	38.8	61.2	0.5	0.634	0.394	-0.289
3	3	53.2	46.8	1	1.137	0.879	0.120

4	2	71.3	28.7	2	2.484	1.610	1.195
5	1	84.0	16.0	5	5.250	4.762	4.048

^aGeneral Condition: 10 μmol Cat. Y, 10 μmol [Ph₃C][B(C₆F₅)₄], 100 μmol Al^tBu₃, Solvent: 50 mL Tol., Temperature: 20 °C. (Conversion of the comonomers < 5 %). ^bDetermined by ¹H and ¹³C NMR spectroscopy.

Intermittent experiment

Table S3: Copolymerization of IP and 2,5-FMOS under different reaction time^a

Entry	Time(h)	Conv.of	Conv.of	2,5-FMOS cont.in	$M_n(10^4)^c$	M_w/M_n^c	$T_g(\text{°C})^d$
		2,5-FMOS (%)	IP (%)	copolymer(mol %) ^b			
1	0.5	9	7	53	2.4	1.14	53
2	1	20	18	52	2.6	1.27	55
3	1.5	26	24	52	4.0	1.17	55
4	2	33	28	54	4.5	1.21	55
5	2.5	39	31	55	4.9	1.16	61
6	3	44	37	55	6.3	1.23	58
7	4	52	42	55	6.7	1.19	63
8	5	61	45	57	7.2	1.18	63
9	6	71	51	58	8.9	1.21	64
10	7	84	59	58	9.5	1.20	65
11	8	92	64	59	10.0	1.16	63

^aGeneral Condition: 10 μmol Cat. Y, 10 μmol [Ph₃C][B(C₆F₅)₄], 100 μmol Al^tBu₃, 2,5-FMOS 3 mmol, IP 3 mmol, Solvent: 1.5 mL Tol., Temperature: 20 °C.

^bDetermined by ¹H and ¹³C NMR spectroscopy. ^cDetermined by gel permeation chromatography in 1,2,4-trichlorobenzene at 150 °C against a polystyrene standard. ^dDetermined by differential scanning calorimetry.

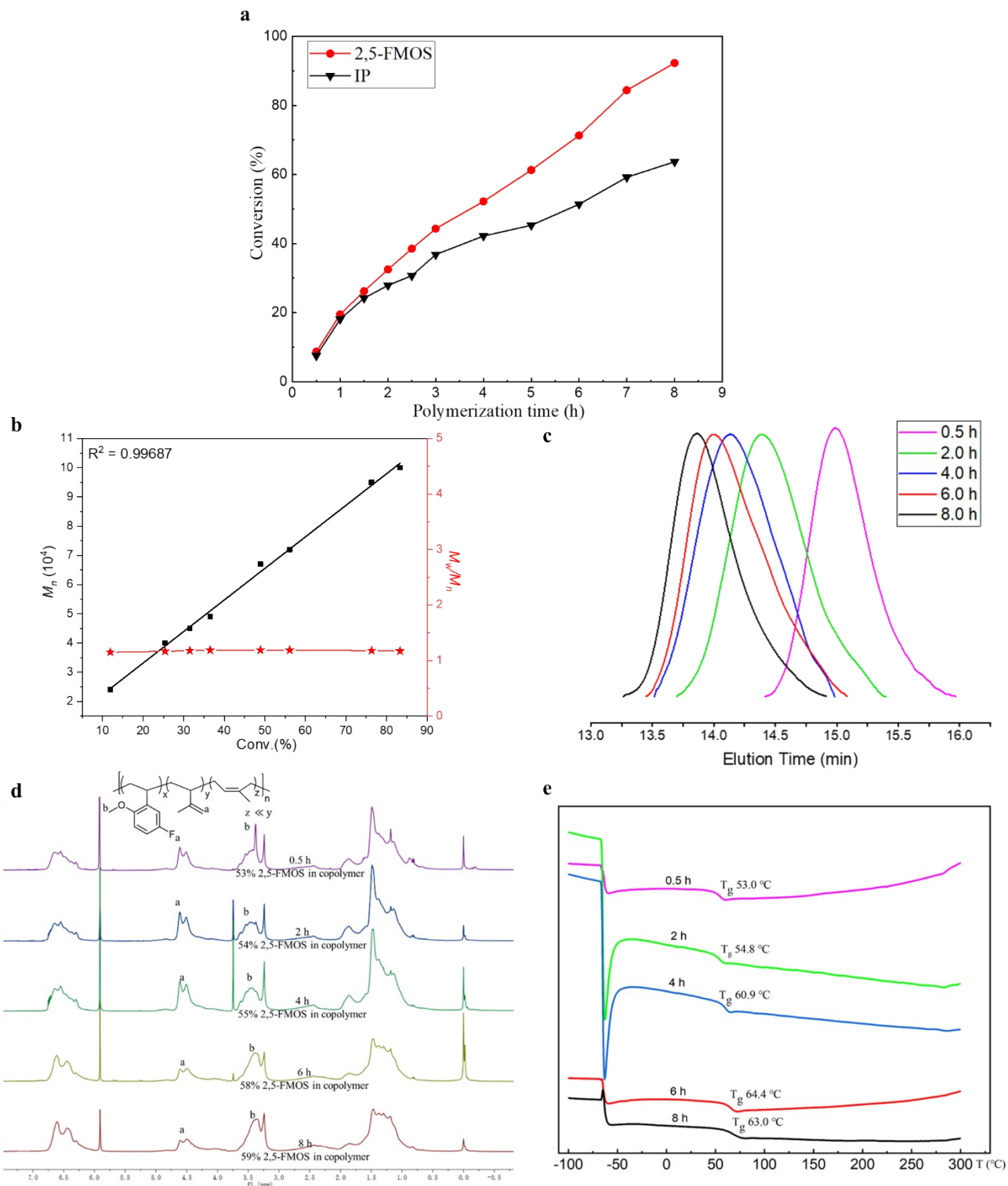


Figure S73. (a) Monomer conversion versus copolymerization time of 2,5-FMOS and IP. (b) Plots of M_n and M_w/M_n against the conversion of monomers. (c) GPC curves of copolymers under different reaction time. (d) ^1H NMR spectrum. (e) DSC curves.

Mechanism of copolymerization of IP and 2,5-FMOS

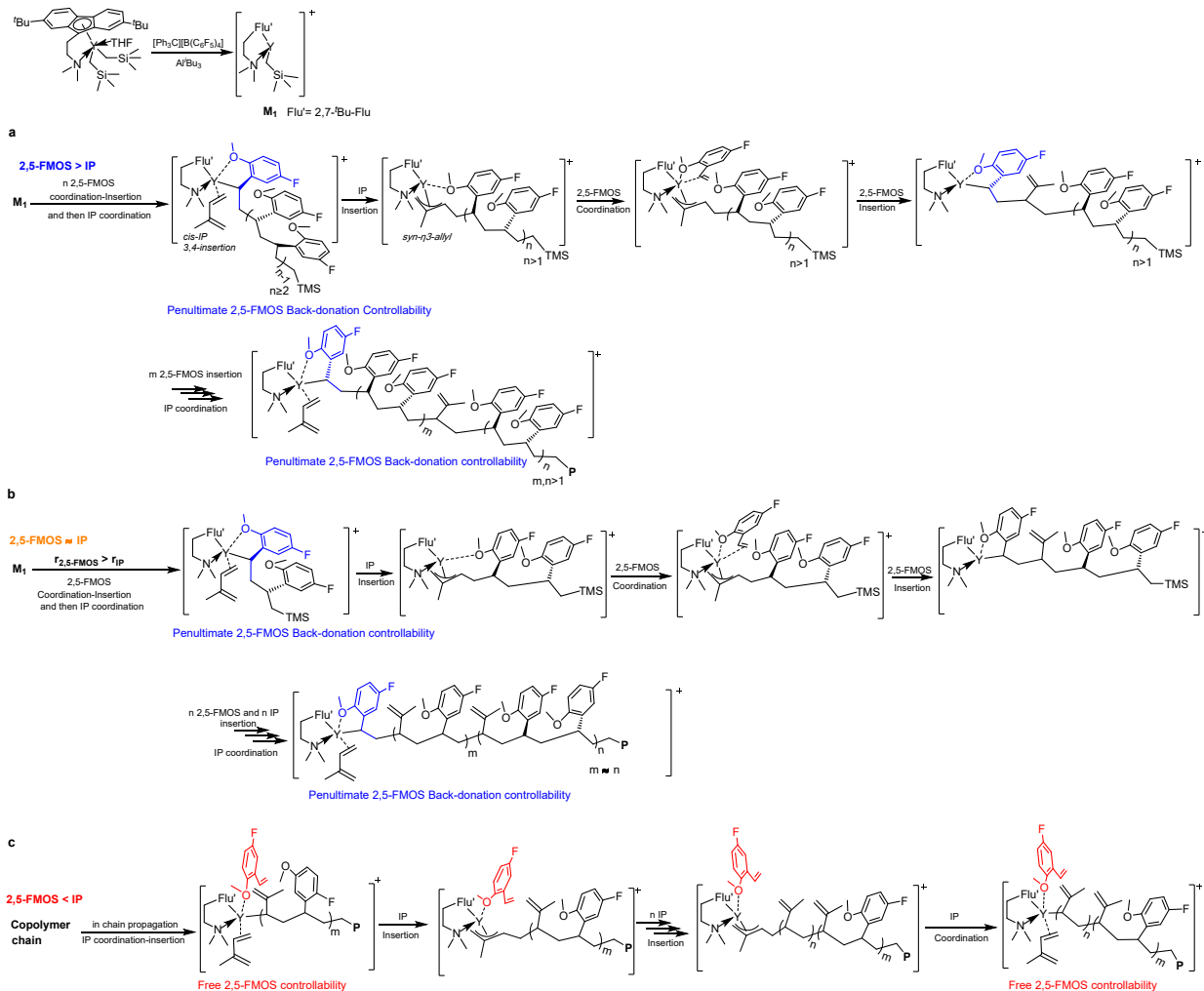


Figure S74. A proposed scenario of copolymerization of IP and 2,5-FMOS. (a) Under high concentration of 2,5-FMOS. (b) Under almost equal concentration of 2,5-FMOS and IP. (c) Under high concentration of IP.

Reference

1. C. Song, J. Chen, Z. Fu, L. Yan, F. Gao, Q. Cao, H. Li, X. Yan, S. Chen, S. Zhang and X. Li, *Macromolecules*, 2021, **54**, 10838-10849.
2. Y. B. Malysheva, S. Combes, A. Y. Fedorov, P. Knochel and A. E. Gavryushin, *Synlett*, 2012, **2012**, 1205-1208.
3. G. W. T. M. J. Frisch, H. B. Schlegel, G. E. Scuseria, M. A. Robb, J. R. Cheeseman, G. Scalmani, V. Barone, G. A. Petersson, H. Nakatsuji, X. Li, M. Caricato, A. V. Marenich, J. Bloino, B. G. Janesko, R. Gomperts, B. Mennucci, H. P. Hratchian, J. V. Ortiz, A. F. Izmaylov, J. L. Sonnenberg, D. Williams-Young, F. Ding, F. Lipparini, F. Egidi, J. Goings, B. Peng, A. Petrone, T. Henderson, D. Ranasinghe, V. G. Zakrzewski, J. Gao, N. Rega, G. Zheng, W. Liang, M. Hada, M. Ehara, K. Toyota, R. Fukuda, J. Hasegawa, M. Ishida, T. Nakajima, Y. Honda, O. Kitao, H. Nakai, T. Vreven, K. Throssell, J. A. Montgomery Jr., J. E. Peralta, F. Ogliaro, M. J. Bearpark, J. J. Heyd, E. N. Brothers, K. N. Kudin, V. N. Staroverov, T. A. Keith, R. Kobayashi, J. Normand, K. Raghavachari, A. P. Rendell, J. C. Burant, S. S. Iyengar, J. Tomasi, M. Cossi, J. M. Millam, M. Klene, C. Adamo, R. Cammi, J. W. Ochterski, R. L. Martin, K. Morokuma, O. Farkas, J. B. Foresman and D. J. Fox, *Gaussian 16, Revision A.03*, Gaussian, Inc., Wallingford, CT, 2016.
4. A. D. Becke, *J. Chem. Phys.*, 1993, **98**, 5648-5652.
5. C. Lee, W. Yang and R. G. Parr, *Phys. Rev. B*, 1988, **37**, 785-789.

6. J. P. Perdew, K. Burke and Y. Wang, *Phys. Rev. B*, 1996, **54**, 16533-16539.
7. P. J. Hay and W. R. Wadt, *J. Chem. Phys.*, 1985, **82**, 270-283.
8. P. J. Hay and W. R. Wadt, *J. Chem. Phys.*, 1985, **82**, 299-310.
9. W. R. Wadt and P. J. Hay, *J. Chem. Phys.*, 1985, **82**, 284-298.
10. A. Höllwarth, M. Böhme, S. Dapprich, A. W. Ehlers, A. Gobbi, V. Jonas, K. F. Köhler, R. Stegmann, A. Veldkamp and G. Frenking, *Chemical Physics Letters*, 1993, **208**, 237-240.
11. Y. Zhao, G. Luo, X. Wang, X. Kang, D. Cui, Z. Hou and Y. Luo, *Organometallics*, 2018, **37**, 3210-3218.
12. Y. Zhao, G. Luo, X. Kang, F. Guo, X. Zhu, R. Zheng, Z. Hou and Y. Luo, *Chem. Commun.*, 2019, **55**, 6689-6692.
13. L. Perrin, F. Bonnet, T. Chenal, M. Visseaux and L. Maron, *Chem-Eur J*, 2010, **16**, 11376-11385.
14. L. Perrin, F. Bonnet, M. Visseaux and L. Maron, *Chem. Commun.*, 2010, **46**, 2965-2967.
15. Y. Zhao and D. G. Truhlar, *Theor. Chem. Acc.*, 2008, **120**, 215-241.
16. Y. Zhao and D. G. Truhlar, *J. Chem. Theory Comput.*, 2009, **5**, 324-333.
17. A. V. Marenich, C. J. Cramer and D. G. Truhlar, *J. Phys. Chem. B*, 2009, **113**, 4538-4543.
18. b. L. CYLview, C. Y., Université de Sherbrooke, 2009 (<http://www.cylview.org>).